

Journal of Sol-Gel Science and Technology

Synthesis and characterization of silver-rich coatings loaded with functionalized clay nanoparticles --Manuscript Draft--

Manuscript Number:	JSST-D-17-00690R1	
Full Title:	Synthesis and characterization of silver-rich coatings loaded with functionalized clay nanoparticles	
Article Type:	Original Paper	
Keywords:	Sol-gel; nanoclays; silver ions; hybrid coating; silver release	
Corresponding Author:	Hugo Fernando Giraldo Mejía Instituto de Investigaciones en Ciencia y Tecnología de Materiales Mar del Plata, Buenos Aires ARGENTINA	
Corresponding Author Secondary Information:		
Corresponding Author's Institution:	Instituto de Investigaciones en Ciencia y Tecnología de Materiales	
Corresponding Author's Secondary Institution:		
First Author:	Hugo Fernando Giraldo Mejía	
First Author Secondary Information:		
Order of Authors:	Hugo Fernando Giraldo Mejía Raúl Ariel Procaccini, Ph. D Sergio Antonio Pellice, Ph. D	
Order of Authors Secondary Information:		
Funding Information:	Consejo Nacional de Investigaciones Científicas y Técnicas	Not applicable
Abstract:	<p>A synthetic exfoliated nanoclay smectite type, Laponite® S482, was incorporated as a functionalized load in a silica hybrid matrix synthesized by the sol-gel route. The previous functionalization was carried out through a "grafting" reaction with (3-glycidioxypropyl)trimethoxysilane (GPTMS) assisted by ultrasonic dispersion. The precursor sols were synthesized by acid-catalyzed hydrolytic condensation between tetraethoxysilane (TEOS) and functionalized GPTMS, a silver ions source was added in order to obtain a coating material with controlled silver releasing properties. Coatings were obtained by "dip-coating" on different substrates. Structural characterization of the coatings was conducted by SAXS and SEM-EDS, the results revealed a complex silica matrix with intercalated nanoclays, an organic fraction and a homogeneous content of Ag⁺. The electrochemical characterization was realized by EIS tests on stainless steel coated substrates AISI 316L type; the results showed good barriers properties and a high integrity of the coatings loaded with nanoclay. The evolution of the release of Ag⁺ ions was studied by XRF, through exposing the coatings to a leaching process at steady state and determining the residual content of Ag within the coat at different immersion times. It was found that the addition of 1.5 wt. % of clay, in respect to condensed silica, decreased the initial diffusion rate of Ag⁺ ions at near the half part, allowing its potential use in the development of antibacterial coatings with longer terms of life.</p>	
Response to Reviewers:	<p>COMMENTS FOR THE AUTHOR:</p> <p>Reviewer #1: A silver-laponite hybrid was synthesized and the silver release from such porous structure was studied. The subject is potentially interesting. But there are some points which should be addressed in the manuscript before any consideration. I suggest major revision of the manuscript based on the following comments:</p> <p>1.The SEM image of silver samples shown in Figure 5a presents some surface cubic</p>	

features very similar to a previous work relating to formation of cubic silver particles (see, J. Phys. D: Appl. Phys. 42 (2009) 105305). The structure of silver particles is important in their interaction with cells and bacteria. This can be further investigated by XRD and its detailed analysis.

response 1:

Thanks for your observation. Certainly, SEM pictures reveals the presence of, likely, cubic silver nanoparticles. XRD spectra reveal the presence of metallic silver in those samples with intensities ratios of the reflection planes (200)/(111) above 0.25 in both cases. As Dr. Akhavan published in J. Phys. D: Appl. Phys. 42 (2009) 105305, such intensities ratios could be certainly attributed to the development of cubic silver nanoparticles. On the other hand, the same article demonstrates that the plasmonic band of such silver nanoparticles, in the UV-visible spectra, have a maximum absorbance around 600 nm. UV-visible spectra, recorded from our silver loaded samples, reveal their maximum intensities around 422 nm. It is important also to have in consideration that SAXS experiments reveals the presence of spherical silver nanoparticles. Probably, in our study, XRD analysis, as SEM pictures, are overlooked by the bigger silver crystals.

The spectroscopic characterization, through XRD and UV-visible, has been added to the manuscript with a discussion and the appropriated references.

2. In Figure 8, the silver release was found around 5h. But, longer release time (~5 days) was also reported (see, for example [Journal of Colloid and Interface Science 336 (2009) 117-124] and [Current Applied Physics 9 (2009) 1381-1385]). Hence the authors should compare the silver release property of this work with the previous ones and discuss about the similarities/differences and advantages/disadvantages. See, for example, Micropor. Mesopor. Mater. 114 (2008) 431 J. Biomed. Mater. Res. 66 (2003) 266 Biomaterials 21 (2000) 393 Dent. Mater. 24 (2008) 1343 Surface and Coatings Technology 203 (2009) 3123-3128 J. Mater. Chem., 2011, 21, 387-393.

Response 2:

Thank you very much for your observation and suggestion. Certainly, comparing the releasing times, it is evident that silver releasing from our samples is considerably faster than the observed in the bibliography that you kindly offer. Such bibliography presents materials with excellent releasing properties and it was introduced in the manuscript. Anyways, it is important take in consideration that antibacterial materials presented in such suggested bibliography have purely inorganic matrixes structures, which are denser than the hybrid organic-inorganic ones. Then it is expectable high differences in the silver releasing results.

Following your kind suggestion, the bibliography and discussion was accordingly enriched in the present version of the manuscript.

3. The chemical state of silver (Ag₀, Ag⁺, and Ag²⁺ states) is very important in its antibacterial activity. This should be studied in the revised version. XPS can be recommended in this regard.

Response 3:

In a previous work [*], we performed XPS measurements in similar coatings thermally treated at the same temperature, 150 °C, and both, Ag⁺ and Ag₀ oxidation states were confirmed. In the chemical system analysed in the present work, we have no argument to assume that silver will behave in a very different way. The high ionic mobility of silver ions and the natural trend of Ag to be reduced drive to the formation of the observed silver particles. Additionally, the results of XRD display, unmistakably, the presence of metallic silver in TGA_g sample and both silver and silver oxide in TGA_g-L1.5% sample. Surely, XPS is a very valuable alternative to elucidate the chemical state of silver in the analysed materials presented in this manuscript. Nevertheless, we consider that this study is beyond the specific objectives of this work and, accordingly, such characterization is in progress and will constitute a next manuscript.

Alternatively, thanks to your previous observation, incorporation of analysis through XRD and UV-visible spectra offer a great improvement in order to elucidate the aggregation state of silver and its release behaviour in the present version of the manuscript.

[*] R. Procaccini, A. Bouchet, J.I. Pastore, C. Studdert, S. Ceré, S. Pellice, Silver-functionalized methyl-silica hybrid materials as antibacterial coatings on surgical-grade stainless steel, Prog. Org. Coatings. 97 (2016) 28–36.
doi:10.1016/j.porgcoat.2016.03.012.

	<p>4.No Antibacterial test was found in the manuscript. So, the results should be added or the terms relating to antibacterial should be deleted.</p> <p>Response 4:</p> <p>Thanks for your clear observation. Although the ionic mobility and silver release behaviour are usually directly involved in the antibacterial performance of this kind of materials, the results of antibacterial tests are not presented in this manuscript. Those analysis are beyond the primary objective of the present manuscript. Accordingly, every term that could, confusedly, ensure antibacterial behaviour of the materials studied in the present manuscript was deleted or accordingly clarified as potential implications of the presented results on antibacterial performances.</p>
Section/Category:	Functional coatings, thin films and membranes (including deposition techniques)

COMMENTS FOR THE AUTHOR:

Reviewer #1: A silver-laponite hybrid was synthesized and the silver release from such porous structure was studied. The subject is potentially interesting. But there are some points which should be addressed in the manuscript before any consideration. I suggest major revision of the manuscript based on the following comments:

1. The SEM image of silver samples shown in Figure 5a presents some surface cubic features very similar to a previous work relating to formation of cubic silver particles (see, J. Phys. D: Appl. Phys. 42 (2009) 105305). The structure of silver particles is important in their interaction with cells and bacteria. This can be further investigated by XRD and its detailed analysis.

Thanks for your observation. Certainly, SEM pictures reveals the presence of, likely, cubic silver nanoparticles. XRD spectra reveal the presence of metallic silver in those samples with intensities ratios of the reflection planes (200)/(111) above 0.25 in both cases. As Dr. Akhavan published in J. Phys. D: Appl. Phys. 42 (2009) 105305, such intensities ratios could be certainly attributed to the development of cubic silver nanoparticles. On the other hand, the same article demonstrates that the plasmonic band of such silver nanoparticles, in the UV-visible spectra, have a maximum absorbance around 600 nm. UV-visible spectra, recorded from our silver loaded samples, reveal their maximum intensities around 422 nm. It is important also to have in consideration that SAXS experiments reveals the presence of spherical silver nanoparticles. Probably, in our study, XRD analysis, as SEM pictures, are overlooked by the bigger silver crystals.

The spectroscopic characterization, through XRD and UV-visible, has been added to the manuscript with a discussion and the appropriated references.

2. In Figure 8, the silver release was found around 5h. But, longer release time (~5 days) was also reported (see, for example [Journal of Colloid and Interface Science 336 (2009) 117-124] and [Current Applied Physics 9 (2009) 1381-1385]). Hence the authors should compare the silver release property of this work with the previous ones and discuss about the similarities/differences and advantages/disadvantages. See, for example, Micropor. Mesopor. Mater. 114 (2008) 431 J. Biomed. Mater. Res. 66 (2003) 266 Biomaterials 21 (2000) 393 Dent. Mater. 24 (2008) 1343 Surface and Coatings Technology 203 (2009) 3123-3128 J. Mater. Chem., 2011, 21, 387-393

Thank you very much for your observation and suggestion. Certainly, comparing the releasing times, it is evident that silver releasing from our samples is considerably faster than the observed in the bibliography that you kindly offer. Such bibliography presents materials with excellent releasing properties and it was introduced in the manuscript. Anyways, it is important take in consideration that antibacterial materials presented in such suggested bibliography have purely inorganic matrixes structures, which are denser than the hybrid organic-inorganic ones. Then it is expectable high differences in the silver releasing results.

Following your kind suggestion, the bibliography and discussion was accordingly enriched in the present version of the manuscript.

3. The chemical state of silver (Ag^0 , Ag^+ , and Ag^{2+} states) is very important in its antibacterial activity. This should be studied in the revised version. XPS can be recommended in this regard.

In a previous work [*], we performed XPS measurements in similar coatings thermally treated at the same temperature, 150 °C, and both, Ag^+ and Ag^0 oxidation states were confirmed. In the chemical system analysed in the present work, we have no argument to assume that silver will behave in a very different way. The high ionic mobility of silver ions and the natural trend of Ag to be reduced drive to the formation of the observed silver particles. Additionally, the results of XRD display, unmistakably, the presence of metallic silver in TGAg sample and both silver and silver oxide in TGAg-L_{1.5%} sample.

Surely, XPS is a very valuable alternative to elucidate the chemical state of silver in the analysed materials presented in this manuscript. Nevertheless, we consider that this study is beyond the specific objectives of this work and, accordingly, such characterization is in progress and will constitute a next manuscript.

Alternatively, thanks to your previous observation, incorporation of analysis through XRD and UV-visible spectra offer a great improvement in order to elucidate the aggregation state of silver and its release behaviour in the present version of the manuscript.

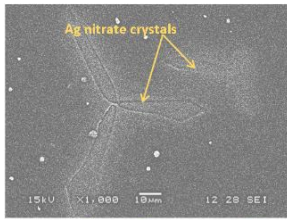
[*] R. Procaccini, A. Bouchet, J.I. Pastore, C. Studdert, S. Ceré, S. Pellice, Silver-functionalized methyl-silica hybrid materials as antibacterial coatings on surgical-grade stainless steel, *Prog. Org. Coatings*. 97 (2016) 28–36. doi:10.1016/j.porgcoat.2016.03.012.

4. No Antibacterial test was found in the manuscript. So, the results should be added or the terms relating to antibacterial should be deleted.

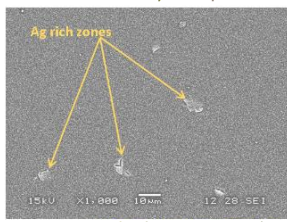
Thanks for your clear observation. Although the ionic mobility and silver release behaviour are usually directly involved in the antibacterial performance of this kind of materials, the results of antibacterial tests are not presented in this manuscript. Those analysis are beyond the primary objective of the present manuscript. Accordingly, every term that could, confusedly, ensure antibacterial behaviour of the materials studied in the present manuscript was deleted or accordingly clarified as potential implications of the presented results on antibacterial performances.

Graphical Abstract

Ag precipitation at Room Temperature (RT) (without Thermal Treatment)

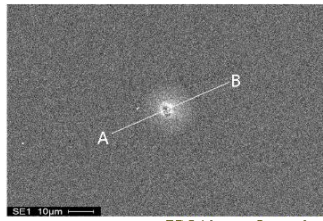


without Clay nanoparticles

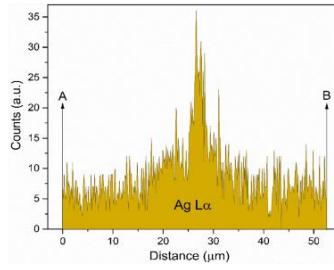


with Clay nanoparticles

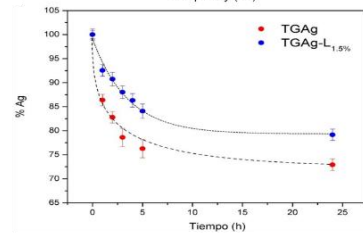
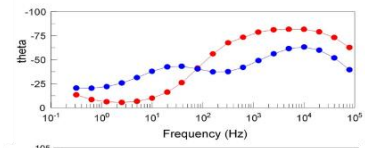
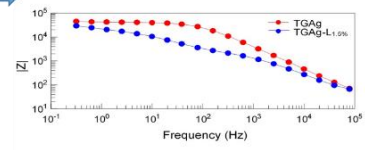
Ag precipitation at 150 °C (30' drying at RT)



EDS Linear Scanning



Electrochemical & Releasing properties



[Click here to view linked References](#)

1

Synthesis and characterization of silver-rich coatings loaded with functionalized clay nanoparticles

Hugo Fernando Giraldo Mejía*, Raúl Ariel Procaccini; Sergio Antonio Pellice

Instituto de Investigación en Ciencia y Tecnología de Materiales (INTEMA), CONICET-UNMdP, Av. Colón 10850, B7606BVZ Mar del Plata, Buenos Aires.

*Corresponding author: Hugo Fernando Giraldo Mejía

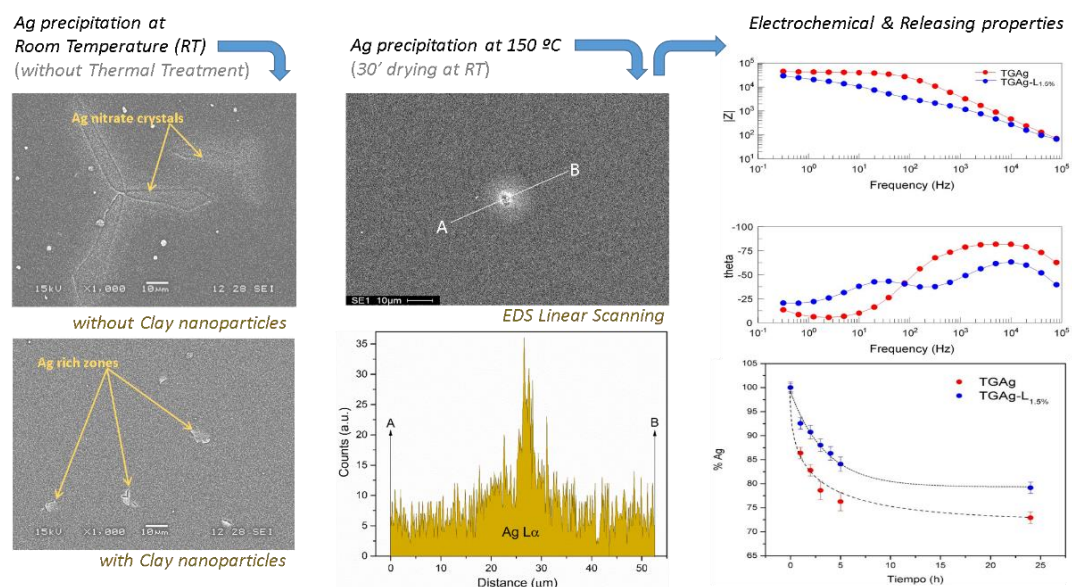
E-mail address: hgiraldo@fi.mdp.edu.ar. Postal address: Av. Juan B. Justo 4302, B7608FDQ Mar del Plata, Argentina. Telephone: +54 223 4816600, extension: 238. ORCID ID: orcid.org/0000-0001-7421-6347.

Abstract

A synthetic exfoliated nanoclay smectite type, Laponite® S482, was incorporated as a functionalized load in a silica hybrid matrix synthesized by the sol-gel route. The previous functionalization was carried out through a "grafting" reaction with (3-glycidoxypropyl)trimethoxysilane (GPTMS) assisted by ultrasonic dispersion. The precursor sols were synthesized by acid-catalyzed hydrolytic condensation between tetraethoxysilane (TEOS) and functionalized GPTMS, a silver ions source was added in order to obtain a coating material with **controlled silver releasing** properties. Coatings were obtained by "dip-coating" on different substrates. Structural characterization of the coatings was conducted by SAXS and SEM-EDS, the results revealed a complex silica matrix with intercalated nanoclays, an organic fraction and a homogeneous content of Ag⁺. The electrochemical characterization was realized by EIS tests on stainless steel coated substrates AISI 316L type; the results showed good barriers properties and a high integrity of the coatings loaded with nanoclay. The evolution of the release of Ag⁺ ions was studied by XRF, through exposing the coatings to a leaching process at steady state and determining the residual content of Ag within the coat at different immersion times. **It was found that the addition of 1.5 wt. % of clay, in respect to condensed silica, decreased the initial diffusion rate of Ag⁺ ions at near the half part, allowing its potential use in the development of antibacterial coatings with longer terms of life.**

Keywords: sol-gel; nanoclays; silver ions; **hybrid coating**; silver release.

Graphical Abstract



1. Introduction

The development of thin coatings through the sol-gel chemistry has reached a huge range of applications that deals with the optical requirements, corrosive processes, energy storage and biologic functionalities among others. In many cases, the coating functionality works on basis of the ionic diffusion through the sol-gel structure. In this sense, the control of such ionic mobility is highly encouraged to ensure an optimum behavior of the functional film.

The diffusive properties of sol-gel coatings can be substantially improved by controlling the crosslinking density of its structure or by incorporation of denser nanoparticles that, at the same time, work as mechanical reinforcement [1, 2]. Certainly, in recent years, the development of new nanocomposites was highly explored by the use of nanoclays thanks to its highly availability and economical convenience. Those nanoparticles are highly employed as rheological modifiers in the industry of cosmetic and paints and, at the same time, their use as load for composite materials can improve both the mechanical and diffusive properties [3–5]. However, the use of clay nanoparticles in the field of sol-gel thin coatings is an area that has not been extendedly analyzed [6–8]. The synthesis of a sol with an appropriated load of well-exfoliated clay nanoparticles, and its deposition as a thin coating, could carry to the development of a high performance sol-gel material. Recently, Santana et al. developed an anticorrosive coating that take the advantage of exfoliated clay nanoparticles to enhance the self-healing performance of cerium-doped sol-gel films [9]. In the field of antibacterial coatings, the same mechanism of diffusion control could be applied to extend to longer terms its capacity through avoiding an unnecessarily excessive releasing of the antibacterial compound. Silver is a well-known biocide component due to the activity of Ag^+ ions [10–14]. Silver ions have an effective action against bacteria life inhibiting their DNA replication process, increasing the permeability of the cytoplasmic membrane and inhibiting the respiratory enzymes, causing asphyxia of the bacteria. So, the development of silver based coatings is in focus for the prevention of periprosthetic infections in surgical prosthesis and orthopedic devices [15–20].

In this work, the study of the effect of exfoliated clay nanoparticles on the thermal evolution and on the silver release behavior of hybrid organic-inorganic sol-gel coatings was addressed. The resulting relationship between the aggregation state of silver and the structure of the hybrid matrix was also studied. Using a synchrotron radiation source, Small Angle X-ray Scattering (SAXS) was performed to analyze the physical structure of the hybrid matrix as a function of the temperature of the thermal treatment. The developed coatings were also analyzed by Electrochemical Impedance Spectroscopy (EIS) and scanning electron microscopy with energy dispersive X-ray spectrometry (SEM/EDS), while the silver release behavior was studied through X-ray fluorescence (XRF) along immersion time.

2. Experimental

Hybrid organic-inorganic sols [2] were synthesized in order to analyze the silver releasing behavior of hybrid coatings with a stratified laminar structure: a base epoxy-silica hybrid sol enriched with ionic silver [TGAg] and sols with the same composition and loaded with different amounts of laminar nanoparticles [TGAg- L_x]. Hybrid sols were synthesized from the hydrolytic condensation of tetraethoxysilane (TEOS, Aldrich 99%) and glycidoxypropil-trimtoxysilane (GPTMS, Aldrich 98%) in acidic media using concentrated HNO_3 as catalyzer. In order to incorporate the laminar nanoparticles in the precursor solution, hydrolysis of TGAg- L_x sols was performed in presence of an aqueous suspension of synthetic exfoliated clay nanoparticles (Laponite[®] S482, Rockwood Specialties, Inc.). AgNO_3 salt was used as supplier of silver. In every case, TEOS/GPTMS molar ratio was kept to 60/40, Laponite was incorporated at a 0.5, 1.0 and 1.5 wt. % in respect to condensed silica and Ag^+ was added, from silver nitrate, to attain an Ag/Si molar ratio of 3/97. Precursor sols were deposited by the dip coating process on AISI 316L stainless steel and glass plates. After deposition, a group of coated substrates was subjected to a drying period of seven days at room temperature without thermal treatment, and other group was thermally treated up to 150 °C in air atmosphere during 1 hour, with a previous shorter drying time (30 minutes) .

Morphology of the obtained coatings, on glass substrates, was analyzed through scanning electron microscopy and energy dispersive X-ray spectrometry (SEM/EDS, Jeol 6460, Japan).

X-ray powder diffraction (XRD) analysis was performed on a X-ray diffractometer (XRD, X'Pert PRO, PANalytical) equipped with a back monochromator and a copper cathode as the X-ray source ($\lambda = 0.154$ nm). Diffractograms were recorded at a speed of 2 °/mm with a counting time of 5 seconds for step.

Silver-enriched coatings were analyzed with an ultraviolet-visible spectrophotometer (UV-Vis-NIR, Shimadzu 3600Plus) equipped with integrating sphere. Spectra were recorded in absorbance mode in the wavelength range from 200 to 1000 nm, with a resolution of 1 nm, using barium sulfate as reflexivity standard.

Electrochemical behavior of the hybrid-coated AISI 316L samples was evaluated by means of electrochemical impedance spectroscopy (EIS) measurements in 0.35 wt. % NaCl solution prepared from p.a. grade chemicals (Sigma-Aldrich) and bidistilled water (Millipore, 18.2 M Ω cm). All measurements were carried out at room temperature (20 ± 1 °C) using a typical three-electrode configuration, with a saturated calomel electrode (SCE, Radiometer Analytical, France) as the reference electrode, a platinum wire of convenient area as counter electrode and the material to be tested as the working electrode. The latter was placed at the bottom of the cell, exposing an area of 3.54 cm². Electrochemical impedance spectroscopy (EIS) was performed at sweeping frequencies from 100 kHz to 0.1 Hz and modulating 10 mV (rms) around the corrosion potential (E_{corr}). EIS fitting was performed using ZView software and EIS conventional theories [21, 22]. All electrochemical potentials in this work are referred to the saturated calomel electrode (0.241 vs. standard hydrogen electrode, SHE).

The release profile of silver ions through both types of consolidated coating matrices was analyzed by X-ray fluorescence spectroscopy (XRF spectrometer, PANalytical Minipal). With the aim of determining the rate of release of Ag⁺ ions over time, leaching stationary tests were carried out in deionized water at constant temperature (30°C) setting the initial content of AgNO₃ at $[\text{Ag}^+]_0 = 3\%$ and a fixed area/volume ratio of approximately 0.2 cm² mL⁻¹ with samples of 6 cm². The obtained XRF spectra made it possible to verify the release capacity of Ag⁺ ions over time by deconvolution of the characteristic signal for Ag L_{α1} (2.98 keV) and subsequent construction of leaching profiles over time.

The structural evolution of the hybrid matrix was analyzed by Small Angle X-ray Scattering (SAXS), as a function of the thermal treatment; the experiments were carried out using the SAXS1 beamline of the National Laboratory of Synchrotron Light (LNLS, Campinas, Brazil). Coatings were taken out from glass substrates by mechanical scratching. The resulting glassy powder was placed in the sample holders by adhesive polyimide film (Kapton®, DuPont). In order to subtract the contribution of the adhesive tape from SAXS patterns, Kapton® film was used as background. The collimated beam crossed the samples through an evacuated flight tube and was scattered to 2D bump-bonded hybrid-pixel Pilatus detector with an active area of 28 cm² and pixel size of 172 × 172 μm². The geometrical configuration was set up with the sample detector distance of 473.5 mm with monochromatic light of $\lambda = 1.55$ Å. The q range was calibrated with silver behenate, which has a well-known lamellar structure with $d = 5.848$ nm [23]. The isotropic 2D scattering patterns were collected after exposure times of 10 s. Images were corrected taking into account the detector dark noise and normalized by the sample transmission considering the 360 azimuthal scan. This procedure was carried out using the FIT2D software [24].

3. Results and discussion

3.1. Structural characterization

Scanning electron microscopy was utilized to analyze the microstructure of *as-received* clay nanoparticles and to verify its ability to exfoliation in aqueous media in order to expose its lamellar structures to further silanization with alkylalkoxides. Figure 1 shows the microstructures of both *as-received* clay nanoparticles and its stratified arrangement achieved after an exfoliation and re-precipitation process in water solution.

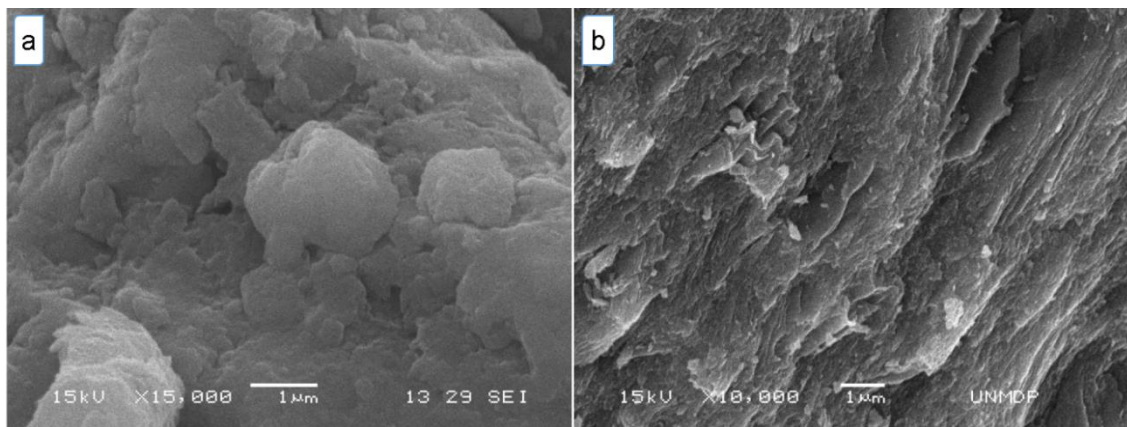


Fig. 1 Scanning Electron Microscopy of Laponite® S482 *a)* as-received and *b)* stratified after its exfoliation in water and a re-precipitation process

With the aim of determine the effect of thermal treatment and the hybrid structure of sol-gel coatings on the aggregation state and stability of Ag^+ ions, small angle x-ray scattering analysis and scanning electron microscopy were performed on TGAg samples dried at 50 °C and thermally densified at 100 and 150 °C. Figure 2 shows the obtained SAXS curves in the region $0.24 < q < 5.2 \text{ nm}^{-1}$, while Figure 2 shows the SEM micrograph of the TGAg coating surface and the image obtained from backscattered electrons.

SAXS curves present, on one hand, a wide and stable peak at 3.7 nm^{-1} characteristic of hybrid organic-inorganic sol-gel structures with a bi-continuous spinodal-like phase separation [25, 26]. On the other hand, a shoulder below 1 nm^{-1} is also observed. This shoulder is attributed to the presence of a polydisperse distribution of spherical silver nanoparticles with a radius of gyration lower than 5 nm. It is clearly observed that the shoulder diminishes and shifts to lower q values for samples densified at higher temperatures because of silver nanoparticles growing.

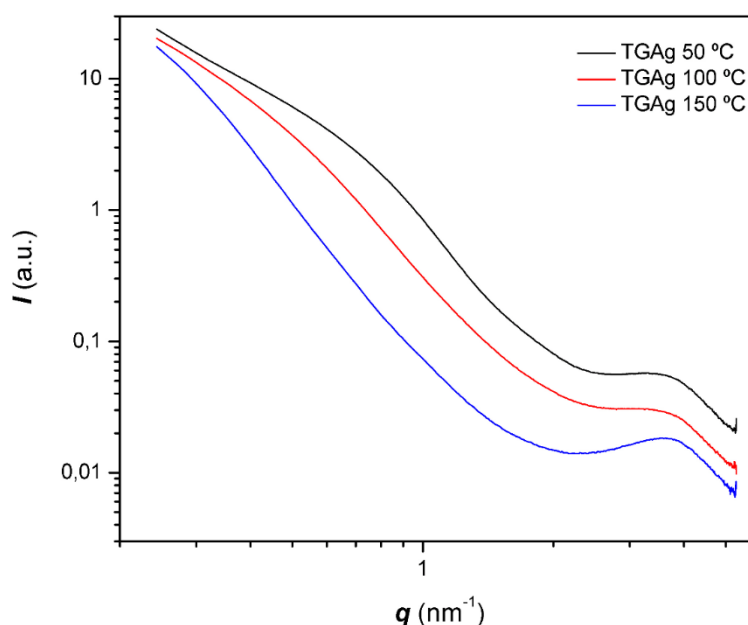


Fig. 2 SAXS curves of TGAg coatings treated at different temperatures.

SEM micrographs of TGAg coatings (Figure 3), revealed, in case of samples stored at room temperature and without thermal densifying treatment, a precipitation of bladed crystalline structures, growing in a three member star-like formation. The image obtained from backscattered electrons (Fig. 3 b) and the EDAX microanalysis (Table 1) revealed the composition of its silver-rich zones.

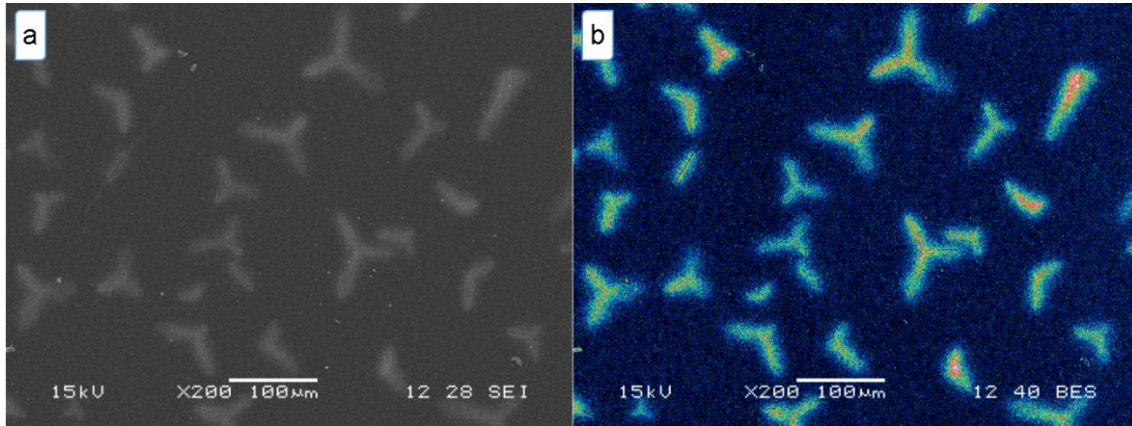


Fig. 3 *a)* SEM micrograph of TGAg coating stored at RT, without thermal treatment, and *b)* image obtained from backscattered electrons.

Table 1 shows the quantitative results of the EDAX microanalysis on different zones of both TGAg and TGAg-L samples showed in the figure 4. A silver segregation effect is observed, since the matrix surrounding the crystals has a lower content of total silver compared than the surface crystals. This can be confirmed in Figure 4 a, where almost 98% of the total silver content are embedded in the crystalline structures of TGAg sample. Whereas for the TGAg-L_{1.5%} type sample (Fig. 4 b) a much lower segregation is observed with some Ag-rich zones with three times higher atomic percent of silver, but with less amount of zones and smaller area than the bladed crystalline structures in TGAg samples. In this case, the matrix with added Laponite® S482 can be considered much more homogeneous, being this a direct effect of the addition of nanoclay in the morphology of the material. It is noteworthy that, in both cases, with and without Laponite® S482, long drying periods carried to the development of structural defects in coatings due to the easy ionic mobility, producing silver segregation with corresponding formation of precipitates.

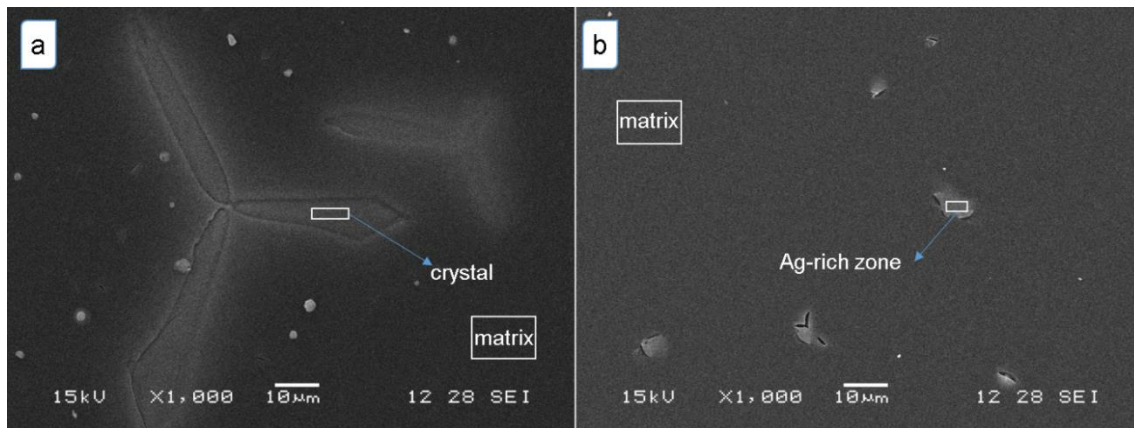


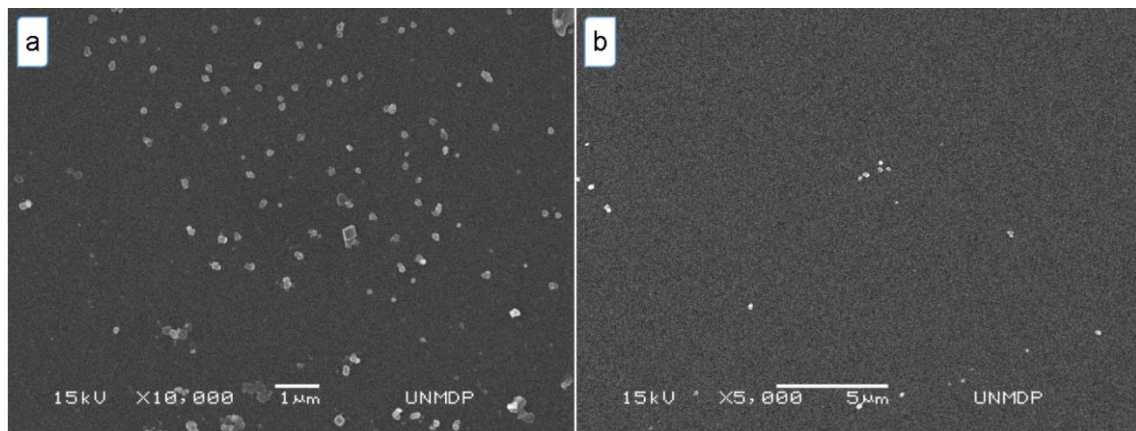
Fig. 4 *a)* SEM micrograph of crystal formation on TGAg coating stored 7 days at RT without thermal treatment and *b)* SEM micrograph of TGAg-L_{1.5%} coating stored 7 days at RT displaying Ag-rich zones.

Table 1: EDAX microanalysis of TGAg and TGAg-L_{1.5%} samples stored at RT without thermal treatment.

Element (At. %)	TGAg (RT)		TGAg-L _{1.5%} (RT)	
	Crystal	Matrix	Ag-rich zone	Matrix
C	31.14	26.76	30.93	34.13
O	33.34	39.84	37.38	37.09
Si	28.24	29.93	24.87	24.96
Na	1.71	1.12	3.22	1.48
Ca	0.90	0.87	1.07	0.92
Ag	2.37	0.05	1.02	0.35

SEM images of Figure 5 from TGAg and TGAg-L_{1.0} samples densified at 150 °C, present homogeneous structures, without the development of bladed crystalline structures or Silver-rich zones. Presumably, the thermal consolidation process favored the growing of inner silver particles in both type of hybrid materials, avoiding the development of bigger surface crystalline structures and the agglomeration of Silver-rich deposits in zones around of the defects of the coating. However, nanometric particles were formed in both coatings, with similar morphology but with different amount of particles per area unit, being significantly more visible in the coatings type TGAg (figure 5 a).

In figure 5 b, it can be observed a lower amount of superficial particles on the coating. This phenomenon is related to the presence of clay nanoparticles in TGAg-L_{1.5%} samples. This phenomenon is attributed to the tortuous path effect given by the arrangement of clay nanoparticles in the matrix, which limits the mobility of silver atoms and, consequently, reduces the growing of superficial silver particles during the consolidating thermal treatment.

**Fig. 5** Scanning Electron Microscopy of a) TGAg and b) TGAg-L_{1.5%} surfaces thermally densified at 150 °C.

From the observed nanoparticles through SEM, a faceted geometry, typical of crystalline structures is suggested. Certainly, from silver ions and its surrounding chemical neighbourhood several crystalline structures, as metallic silver, silver oxide or ionic salts, could be expected [27, 28]. X-ray diffractograms of TGAg sample, figure 6 a, besides the broad band attributed to the amorphous matrix of the coating, reveals the presence of peaks at 38.2°, 44.3°, 64.5° and 77.4°, which are attributed to the (111), (200), (220) and (311) reflections planes, respectively, of the face-centered cubic (FCC) structure of metallic silver (JCPDS no. 65-2871). In sample TGAg-L_{1.5%}, the presence of Laponite® S482 produced the appearance of a new crystalline phase with diffraction peaks at 28°, 32.5°, 46.7° 55° and 57°, which are assigned to the reflection planes (110), (111), (200), (220) and (311), respectively, of the cubic phase of Ag₂O (JCPDS no. 76-1393). The development of silver oxide could be attributed, presumably, to an alkalinisation of the composite material during its drying and densification process.

UV-visible spectra of TGAg and TGAg-L_{1.5%} samples, figure 6 b, reveal the effect of clay nanoparticles on the development of silver nanoparticles from its ionic state. Besides the strong

absorbance below 350 nm, attributed to silica bonds, with the densifying thermal treatment Ag^+ ions reduce giving place to the development of the characteristic plasmonic bands attributed to silver nanoparticles. Although in both silver loaded samples the maximum is developed at 422 nm, in TGAg-L_{1.5%} sample, were clay nanoparticles provide a diffusion barrier, the resulting plasmonic band is considerably more intense and narrow than the observed in absence of clay nanoparticles. This phenomenon, evidencing a narrower size distribution and a higher density of silver nanoparticles in clay-containing coatings, could be attributed to a strong limitation of silver ions to migrate inside the nanocomposite coating and grow bigger silver nanoparticles.

Although both SEM pictures and a crystallographic study, performed through the intensities ratios of the reflection planes (200)/(111) of silver nanoparticles, suggest the development of cubic silver nanoparticles [27], it is not the observed by UV-visible spectroscopy. In agreement with the result obtained from SAXS studies, and according to Mie's theory, the development of single surface plasmonic bands suggest the development of mainly spherical nanocrystals of silver; anisotropic particles should exhibit two or three bands, depending on their shape [29]. This inconsistency may be attributed to the presence of bigger silver particles that do not fit to the nanoscale range.

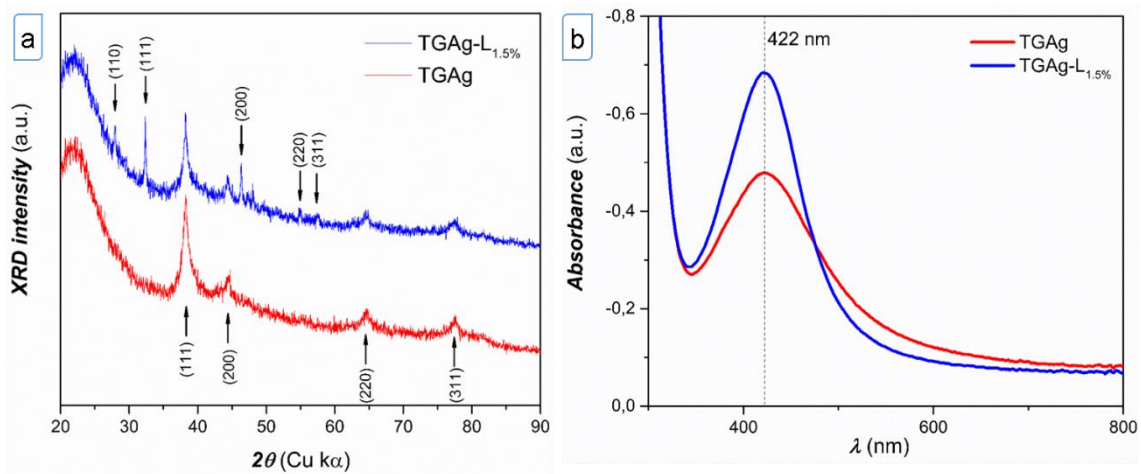


Fig. 6 a) XRD and b) UV-visible spectra of TGAg and TGAg-L_{1.5%} samples thermally densified at 150 °C.

In order to analyze the distribution of silver in the matrix and the Ag rich particles in the consolidated films, an EDAX line scan analysis (Figure 7) was performed. The result shows a homogeneous distribution around the particles, and a concentration of silver in the particle at least three times higher, based on the intensity of the L- α line of Ag atoms in the coating. This distribution of silver concentrations in the coating is similar to that obtained in matrices type TGAg-L_{1.5%} without thermal treatment. Therefore, it can be assumed that, in samples treated at 150 °C with short drying period, the presence of Laponite® S482 also limits the surface particle growth and promotes the homogenization of the silver distribution in the coating.

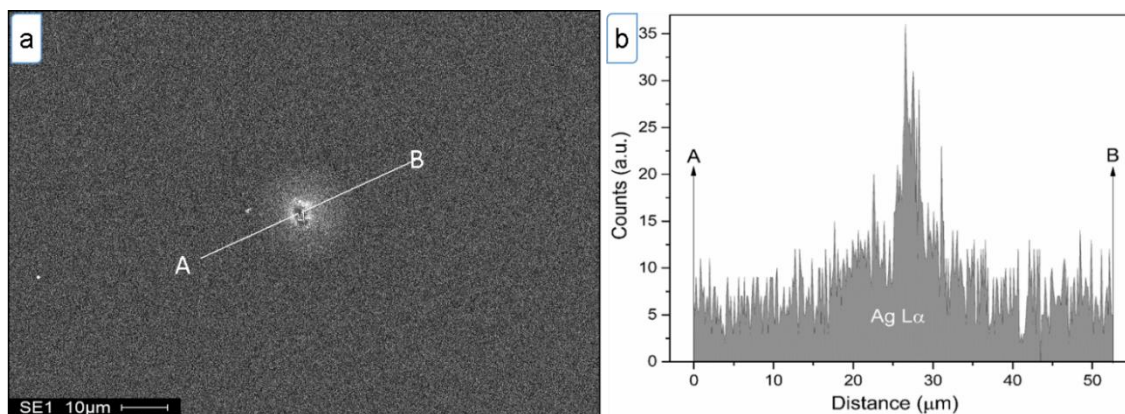


Fig. 7 a) SEM image of a TGAg surface particle and EDAX line scan microanalysis, the white line is the pathway where EDS analysis was performed, and b) Ag L- α line profile in the scan microanalysis.

3.2 Silver release

Capability of silver to be released from the coatings in aqueous media was studied through EIS and lixiviation tests by analysis of silver retained in the coating after different immersion times through XRF.

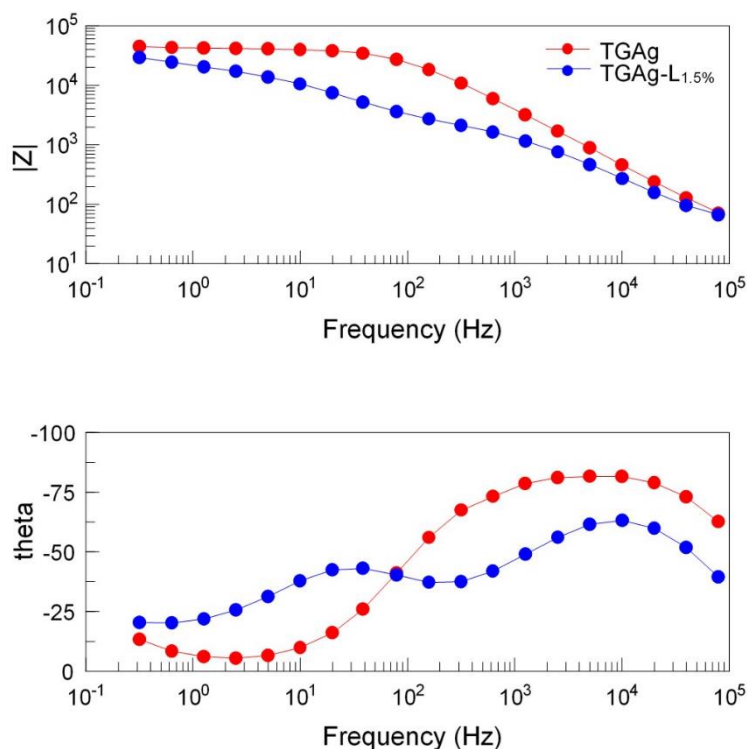


Fig. 8 Bode representation for TGAg (red dots) and TGAg-L_{1.5} (blue dots) coatings exposed at 0.01 mol·L⁻¹ NaCl aerated solution.

Figure 8 shows the EIS results for TGAg and TGAg-L_{1.5} coatings. The nanoclay-free coating reveals a wide curve at high frequencies, related to a high barrier effect, indicating the presence of a continuous and integral coating on the stainless steel substrate [30, 31]. These two time constants, at an angle near to 90°, suggests a dielectric capacitive behavior with some grade of porosity as evidenced in

the decrease of the angle in the low frequency region [32]. Incorporation of clay nanoparticles, as observed for sample TGA_g-L_{1.5%}, becomes the coating less resistive in all the frequencies range tested. In the phase angle representation, incorporation of clay nanoparticles causes the rising of a second time constant at lower frequencies presumably associated to the presence of defects in the coating [33–35]. Moreover, the appearance of the second time constant may be caused by the change in the structure of the matrix due to the presence of nanoclay, causing a reordering of the silver particles.

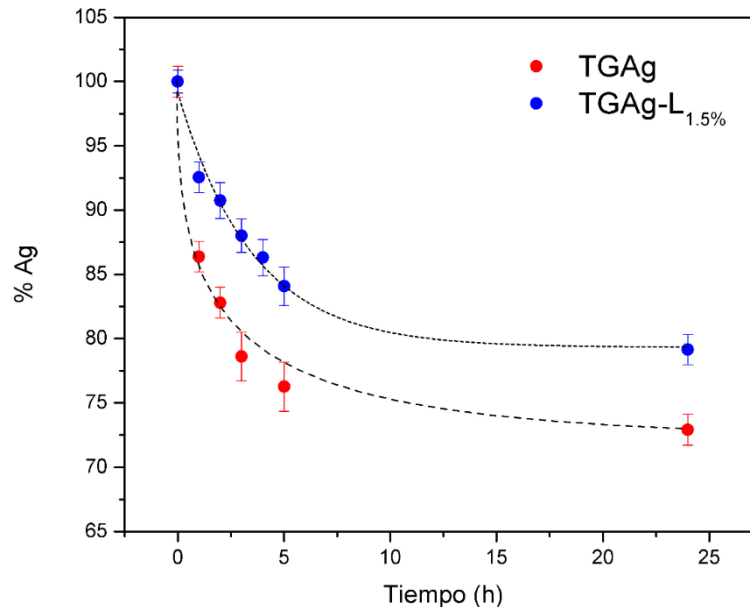


Fig. 9 Curves of silver releasing for TGA_g (red dots) and TGA_g-L_{1.5} (blue dots) samples, subjected to a lixiviation process to different times.

Lixiviation tests show the higher loosening rate of silver during the first hours of immersion for both thermally consolidated samples. Figure 9 displays the lixiviation curves of TGA_g and TGA_g-L_{1.5} samples. In TGA_g coating, the silver releasing process starts, fast, at a rate of 13.5 ± 1.25 %/h. At the 24 hours of immersion, the 27 ± 1.3 % of the silver initially available was released, reaching a stationary state of saturation where the 80% of silver in solution was released in the firsts 3 hours of the test. Incorporation of clay nanoparticles revealed a strong effect on such releasing parameters: the starting rate of silver releasing was of 7.5 ± 1.25 %/h and its stationary sate of saturation was reached at the 6 hours approximately. In this case, only a 20 ± 1.3 % of the initially available silver was released during the 24 hours of immersion.

Leaching results reveal a clear retardant effect produced by the nanoclay addition to the hybrid matrix on the silver mobility and release. This effect can be explained by the tortuous-path provided by the arrangement of the nanoclays into the matrix, to the mobility of silver ions and particles, and the limitation that these introduce to the formation of crystalline and silver-rich deposits on the surface. O. Akhavan [36] found a similar behavior of silver releasing from purely inorganic sol-gel coatings, where the addition of a second layer of titania-based film produced a barrier effect introducing significant changes in time and concentration of saturation. Immobilization of silver ions and nanoparticles in denser structure matrixes allows to obtain longer term releasing properties. So, in cases where silver nanoparticles are imbedded in films based on dense silicon or titanium oxides, or within multi-wall carbon nanotubes, releasing rates are lets to extent lixiviation tests along several days, or weeks, of immersion [37–41]. On the contrary, when the internal structure of the coating, that containing the silver nanoparticles or silver ions, is less dense, due to lower thermal densification temperatures or the introduction of organic components, the leaching of silver proceeds at a much higher rates [42–44].

3.2. Influence of the nanocomposite structure on silver aggregation and mobility.

As could be observed from Figure 2, the epoxy-silica hybrid structure developed from TEOS and GPTMS present, near independently from the densifying thermal treatment, a bi-continuous phase separation whose domains are at the nanometric scale. This structure is highly favorable to make enable the ionic mobility into its structure. On the other hand, the aggregation state of silver is extremely sensitive to the temperature. As temperatures rises, silver ions tend to reduce and aggregate in bigger particles that could carry to a loosening of its antibacterial effect [44, 45]. However, the absence of thermal densifying treatment, beside to maximize the presence of silver ions and small clusters, causes an incomplete silica condensation of the hybrid matrix allowing the recrystallization of silver nitrate. Figure 3 shows the growing of big crystals, rich in silver, inside a hybrid organic-inorganic matrix with barely detectable silver in its atomic composition. It is worthy to note that those developed silver nitrate crystals have a high aspect ratio since the coating is about only 2 μm thickness.

Taking into account the behavior of silver in the epoxy-silica matrix, arises the need to introduce a mobility restraint. Exfoliated clay nanoparticles, as thin sheets with crystalline structure, could diminish the ionic mobility with only a few amounts of exfoliated nanoparticles into thin sol-gel coatings. Incorporation of clay nanoparticles, with a good enough level of exfoliation into the sol-gel matrix, requires its capability to be exfoliated and dispersed in the sol. Moreover, in order to obtain a physicochemically stable sol, isolated clay nanosheets should be organically functionalized to become compatible with its chemical surrounding. The microstructural differences between Laponite particles as-received and its stratified structure after its further re-precipitation from aqueous dispersion, Figure 1, allows to verify its capability to be introduced to the sol-gel composite thanks to the possibility to be dispersed as exfoliated sheets and then, after drying, re-precipitate in a stratified arrangement.

Thus, introduction of clay nanoparticles in the formulation of silver enriched epoxy-silica material was performed obtaining homogeneous coatings. As could be observed through SEM, Figure 4, TGAg-L_{1.5} coatings present a much more homogeneous surface without the strong development of silver particles as in TGAg coatings. Such superficial difference could be indicative of the restrained ionic mobility provided by clay nanoparticles; ionic silver has not enough to reach the external surface of the coating, where silver particles could grow without structural limitations.

Electrochemical tests revealed better barrier properties in coatings without Laponite. This result could be a consequence of the development of a more crosslinked network due to the releasing of silver towards the external surface in clay-free coatings. Nevertheless, as the objective of this kind of coating is to provide a controlled silver release, instead of anticorrosive properties, the presence of such structural defects should not mean a concerning result.

Finally, although coating without clay nanoparticles presented a more crosslinked network, as electrochemical tests revealed, the silver release behavior was considerably restrained with the addition of just 1.5 % of Laponite® S482. Typically, this kind of materials with silver releasing properties, present a huge importance in applications as antibacterial coatings. In such cases, both the capacity of the substrate to tolerate the deposition procedure and the use conditions of the functionalized material will be determining in the selection of coating composition.

4. Conclusions

Exfoliated clay nanoparticles were successfully incorporated in silver-enriched hybrid organic-inorganic thin sol-gel coatings. The hybrid matrix developed from TEOS and GPTMS present a spinodal-like bi-continuous structure which is highly favorable to mobility of silver ions towards the external coating surface, allowing, in certain cases, an unnecessary early silver release.

Besides, to work as a control to silver diffusion, as electrochemical tests suggest, clay nanoparticles have a complementary effect on the silver ions behavior avoiding its losing by superficial agglomeration during the thermal densification of coatings.

Incorporation of just 1.5 wt. % of Laponite® S482, in respect of condensed silica, improved the silver releasing behavior, allowing to extend its term of life five times longer and allows a potential application in the field of antibacterial materials.

Acknowledgements

Authors want to acknowledge the Argentine National Council of Scientific and Technical Researches (CONICET, PIP 2012-0434) and the National Synchrotron Light Laboratory of Brazil (LNLS, Project 6780/10, proposal D11A-SAXS1-15291) for the financial supports. In addition, Mr. Martín E. Lere is gratefully acknowledged for his helpful technical collaboration.

Compliance with Ethical Standards

Conflict of Interest: The authors declare that they have no conflict of interest.

References

1. Schmidt H, Jonschker G, Goedicke S, Mennig M (2000) The Sol-gel process as a basic technology for nanoparticle-dispersed inorganic-organic composites. *J Sol-Gel Sci Technol* 19:39–51. doi: 10.1023/A:1008706003996
2. Pandey S, Mishra SB (2011) Sol-gel derived organic-inorganic hybrid materials: Synthesis, characterizations and applications. *J Sol-Gel Sci Technol* 59:73–94. doi: 10.1007/s10971-011-2465-0
3. Olivier MG, Fedel M, Sciamanna V, et al (2011) Study of the effect of nanoclay incorporation on the rheological properties and corrosion protection by a silane layer. *Prog Org Coatings* 72:15–20. doi: 10.1016/j.porgcoat.2010.11.022
4. Yeh J-M, Chen C-L, Chen Y-C, et al (2002) Enhancement of corrosion protection effect of poly(o-ethoxyaniline) via the formation of poly(o-ethoxyaniline)-clay nanocomposite materials. *Polymer (Guildf)* 43:2729–2736. doi: 10.1016/S0032-3861(02)00005-8
5. Herrera Alonso R, Estevez L, Lian H, et al (2009) Nafion-clay nanocomposite membranes: Morphology and properties. *Polymer (Guildf)* 50:2402–2410. doi: 10.1016/j.polymer.2009.03.020
6. Deflorian F, Rossi S, Fedel M, Motte C (2010) Electrochemical investigation of high-performance silane sol-gel films containing clay nanoparticles. *Prog Org Coatings* 69:158–166. doi: 10.1016/j.porgcoat.2010.04.007
7. Seeni Meera KM, Murali Sankar R, Murali A, et al (2012) Sol-gel network silica/modified montmorillonite clay hybrid nanocomposites for hydrophobic surface coatings. *Colloids Surfaces B Biointerfaces* 90:204–210. doi: 10.1016/j.colsurfb.2011.10.018
8. Joncoux-Chabrol K, Bonino JP, Gressier M, et al (2012) Improvement of barrier properties of a hybrid sol-gel coating by incorporation of synthetic talc-like phyllosilicates for corrosion protection of a carbon steel. *Surf Coatings Technol* 206:2884–2891. doi: 10.1016/j.surfcoat.2011.12.017
9. Santana I, Pepe A, Schreiner W, et al (2015) Hybrid sol-gel coatings containing clay nanoparticles for corrosion protection of mild steel. *Electrochim Acta*. doi: 10.1016/j.electacta.2016.01.214

10. Jones SA, Bowler PG, Walker M, Parsons D (2004) Controlling wound bioburden with a novel silver-containing Hydrofiber?? dressing. *Wound Repair Regen* 12:288–294. doi: 10.1111/j.1067-1927.2004.012304.x
11. Silver S, Phung LT (1996) Bacterial heavy metal resistance: new surprises. *Annu Rev Microbiol* 50:753–89. doi: 10.1146/annurev.micro.50.1.753
12. Crabtree JH, Burchette RJ, Siddiqi RA, et al (2003) The efficacy of silver-ion implanted catheters in reducing peritoneal dialysis-related infections. *Perit Dial Int* 23:368–374.
13. Zhao G, Stevens SE (1998) Multiple parameters for the comprehensive evaluation of the susceptibility of *Escherichia coli* to the silver ion. *BioMetals* 11:27–32. doi: 10.1023/A:1009253223055
14. Ando Y, Miyamoto H, Noda I, et al (2010) Calcium phosphate coating containing silver shows high antibacterial activity and low cytotoxicity and inhibits bacterial adhesion. *Mater Sci Eng C* 30:175–180. doi: 10.1016/j.msec.2009.09.015
15. Sun B, Sun SQ, Li T, Zhang WQ (2007) Preparation and antibacterial activities of Ag-doped SiO₂-TiO₂ composite films by liquid phase deposition (LPD) method. *J Mater Sci* 42:10085–10089. doi: 10.1007/s10853-007-2109-5
16. Jeanmonod P, Laschke MW, Gola N, et al (2014) Early host tissue response to different types of vascular prostheses coated with silver acetate or vaporized metallic silver. *Eur J Vasc Endovasc Surg* 47:680–688. doi: 10.1016/j.ejvs.2014.03.006
17. Ferreri I, Lopes V, Calderon V. S, et al (2014) Study of the effect of the silver content on the structural and mechanical behavior of Ag-ZrCN coatings for orthopedic prostheses. *Mater Sci Eng C* 42:782–790. doi: 10.1016/j.msec.2014.06.007
18. Qin H, Cao H, Zhao Y, et al (2014) In vitro and in vivo anti-biofilm effects of silver nanoparticles immobilized on titanium. *Biomaterials* 35:9114–9125. doi: 10.1016/j.biomaterials.2014.07.040
19. Abboud EC, Settle JC, Legare TB, et al (2014) Silver-based dressings for the reduction of surgical site infection: Review of current experience and recommendation for future studies. *Burns* 40:S30–S39. doi: 10.1016/j.burns.2014.09.011
20. Dal Lago V, França de Oliveira L, de Almeida Gonçalves K, et al (2011) Size-selective silver nanoparticles: future of biomedical devices with enhanced bactericidal properties. *J Mater Chem* 21:12267. doi: 10.1039/c1jm12297e
21. Orazem ME, Tribollet B (2008) *Electrochemical Impedance Spectroscopy*. Analysis. doi: 10.1002/9780470381588
22. McIntyre JM, Pham HQ (1996) Electrochemical impedance spectroscopy; coatings optimizations a tool for organic. *Prog Org Coatings* 27:201–207. doi: 10.1016/0300-9440(95)00532-3
23. Huang TC, Toraya H, Blanton TN, Wu Y (1993) X-ray Powder Diffraction Analysis of Silver Behenate, a Possible Low-Angle Diffraction Standard. *J Appl Crystallogr* 3:180–184. doi: 10.1107/S0021889892009762
24. Hammersley AP (2016) FIT2D: A multi-purpose data reduction, analysis and visualization program. *J Appl Crystallogr* 49:646–652. doi: 10.1107/S1600576716000455
25. Teubner M, Strey R (1987) Origin of the scattering peak in microemulsions. *J Chem Phys* 87:3195–3200. doi: 10.1063/1.453006
26. Laity PR, Taylor JE, Wong SS, et al (2004) A review of small-angle scattering models for random segmented poly(ether-urethane) copolymers. *Polymer (Guildf)* 45:7273–7291. doi: 10.1016/j.polymer.2004.08.033
27. Akhavan O (2009) Silver nanocube crystals on titanium nitride buffer layer. *J Phys D Appl Phys*. doi:

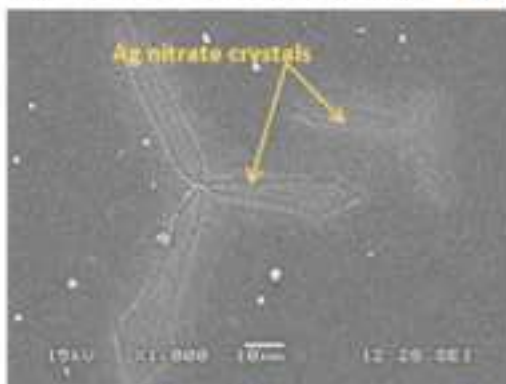
10.1088/0022-3727/42/10/105305

- 1
 - 2
 - 3
 - 4
 - 5
 - 6
 - 7
 - 8
 - 9
 - 10
 - 11
 - 12
 - 13
 - 14
 - 15
 - 16
 - 17
 - 18
 - 19
 - 20
 - 21
 - 22
 - 23
 - 24
 - 25
 - 26
 - 27
 - 28
 - 29
 - 30
 - 31
 - 32
 - 33
 - 34
 - 35
 - 36
 - 37
 - 38
 - 39
 - 40
 - 41
 - 42
 - 43
 - 44
 - 45
 - 46
 - 47
 - 48
 - 49
 - 50
 - 51
 - 52
 - 53
 - 54
 - 55
 - 56
 - 57
 - 58
 - 59
 - 60
 - 61
 - 62
 - 63
 - 64
 - 65
28. Fang J, Leufke PM, Kruk R, et al (2010) External electric field driven 3D ordering architecture of silver (I) oxide meso-superstructures. *Nano Today* 5:175–182. doi: 10.1016/j.nantod.2010.05.002
29. Dhoondia ZH, Chakraborty H (2012) *Lactobacillus* Mediated Synthesis of Silver Oxide Nanoparticles. *Nanomater Nanotechnol* 2:15. doi: 10.5772/55741
30. Zheng S, Li J (2010) Inorganic-organic sol gel hybrid coatings for corrosion protection of metals. *J Sol-Gel Sci Technol* 54:174–187. doi: 10.1007/s10971-010-2173-1
31. Balgude D, Sabnis A (2012) Sol-gel derived hybrid coatings as an environment friendly surface treatment for corrosion protection of metals and their alloys. *J Sol-Gel Sci Technol* 64:124–134. doi: 10.1007/s10971-012-2838-z
32. Carmezim MJ, Simões AM, Montemor MF, Da Cunha Belo M (2005) Capacitance behaviour of passive films on ferritic and austenitic stainless steel. In: *Corros. Sci.* pp 581–591
33. Yasakau KA, Zheludkevich ML, Karavai O V., Ferreira MGS (2008) Influence of inhibitor addition on the corrosion protection performance of sol-gel coatings on AA2024. *Prog Org Coatings* 63:352–361. doi: 10.1016/j.porgcoat.2007.12.002
34. Liu C, Bi Q, Leyland A, Matthews A (2003) An electrochemical impedance spectroscopy study of the corrosion behaviour of PVD coated steels in 0.5 N NaCl aqueous solution: Part II.: EIS interpretation of corrosion behaviour. *Corros Sci* 45:1257–1273. doi: 10.1016/S0010-938X(02)00214-7
35. Mansfeld F (1995) Use of electrochemical impedance spectroscopy for the study of corrosion protection by polymer coatings I ---I I. *J Appl Electrochem* 25:187–202. doi: 10.1007/BF00262955
36. Akhavan O (2009) Lasting antibacterial activities of Ag-TiO₂/Ag/a-TiO₂ nanocomposite thin film photocatalysts under solar light irradiation. *J Colloid Interface Sci* 336:117–124. doi: 10.1016/j.jcis.2009.03.018
37. Akhavan O, Ghaderi E (2009) Bactericidal effects of Ag nanoparticles immobilized on surface of SiO₂ thin film with high concentration. *Curr Appl Phys* 9:1381–1385. doi: 10.1016/j.cap.2009.03.003
38. Liu Y, Wang X, Yang F, Yang X (2008) Excellent antimicrobial properties of mesoporous anatase TiO₂ and Ag/TiO₂ composite films. *Microporous Mesoporous Mater* 114:431–439. doi: 10.1016/j.micromeso.2008.01.032
39. Kawashita M, Toda S, Kim H-M, et al (2003) Preparation of antibacterial silver-doped silica glass microspheres. *J Biomed Mater Res* 66A:266–274. doi: 10.1002/jbm.a.10547
40. Akhavan O, Abdolhad M, Abdi Y, Mohajerzadeh S (2011) Silver nanoparticles within vertically aligned multi-wall carbon nanotubes with open tips for antibacterial purposes. *J Mater Chem* 21:387–393. doi: 10.1039/C0JM02395G
41. Akhavan O, Ghaderi E (2009) Capping antibacterial Ag nanorods aligned on Ti interlayer by mesoporous TiO₂ layer. *Surf Coatings Technol* 203:3123–3128. doi: 10.1016/j.surfcoat.2009.03.033
42. Mahltig B, Fiedler D, Böttcher H (2004) Antimicrobial Sol – Gel Coatings. *J Sol-Gel Sci Technol* 32:219–222.
43. Stobie N, Duffy B, McCormack DE, et al (2008) Prevention of *Staphylococcus epidermidis* biofilm formation using a low-temperature processed silver-doped phenyltriethoxysilane sol-gel coating. *Biomaterials* 29:963–969. doi: 10.1016/j.biomaterials.2007.10.057
44. Procaccini RA, Studdert CA, Pellice SA (2014) Silver doped silica-methyl hybrid coatings. Structural evolution and antibacterial properties. *Surf Coatings Technol* 244:92–97. doi: 10.1016/j.surfcoat.2014.01.036

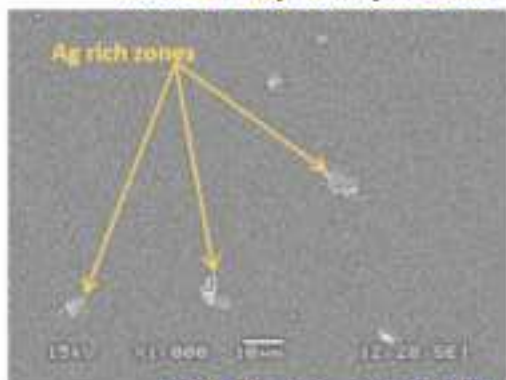
45. Procaccini R, Bouchet A, Pastore JJ, et al (2016) Silver-functionalized methyl-silica hybrid materials as antibacterial coatings on surgical-grade stainless steel. *Prog Org Coatings* 97:28–36. doi: 10.1016/j.porgcoat.2016.03.012

1
2
3
4
5
6
7
8
9
10
11
12
13
14
15
16
17
18
19
20
21
22
23
24
25
26
27
28
29
30
31
32
33
34
35
36
37
38
39
40
41
42
43
44
45
46
47
48
49
50
51
52
53
54
55
56
57
58
59
60
61
62
63
64
65

**Ag precipitation at
Room Temperature (RT)
(without Thermal Treatment)**

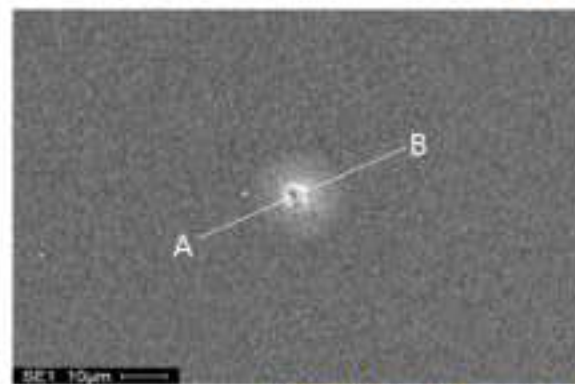


without Clay nanoparticles

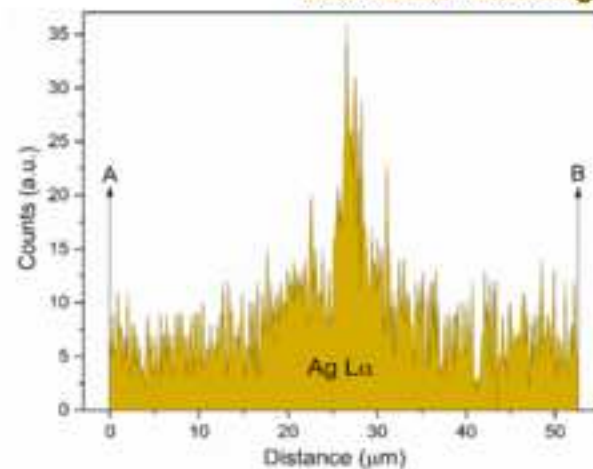


with Clay nanoparticles

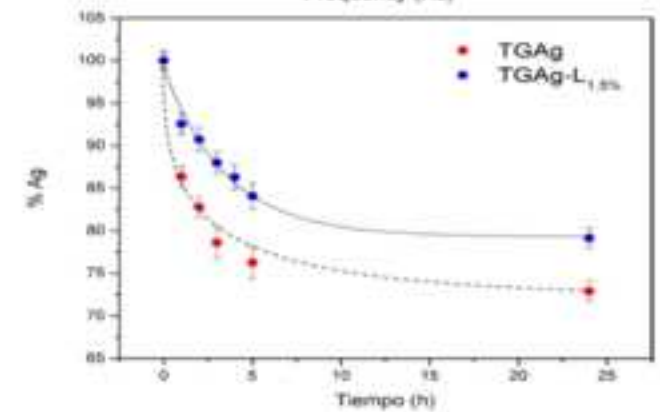
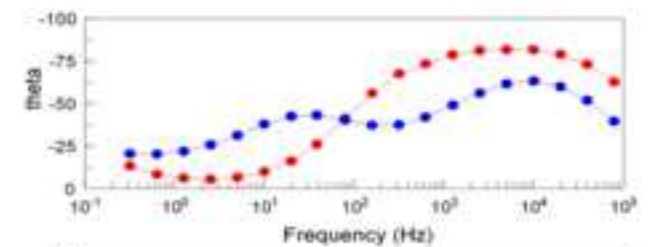
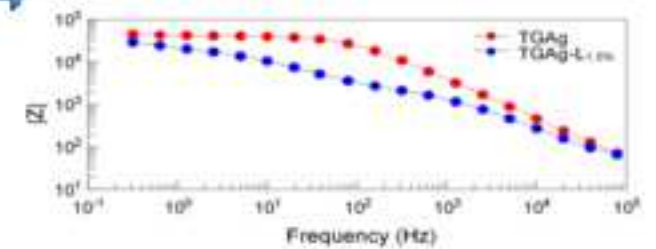
**Ag precipitation at 150 °C
(90' drying at RT)**

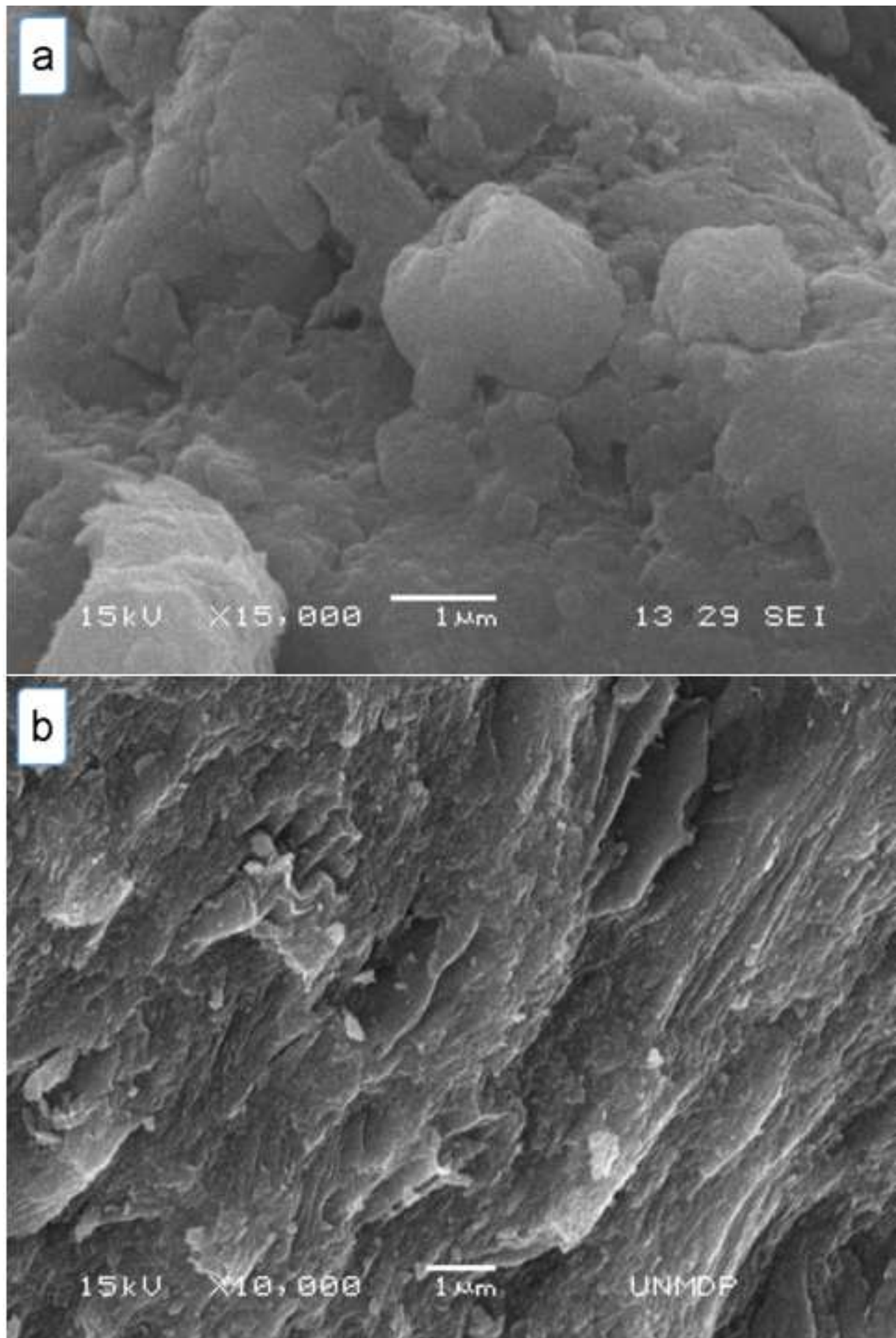


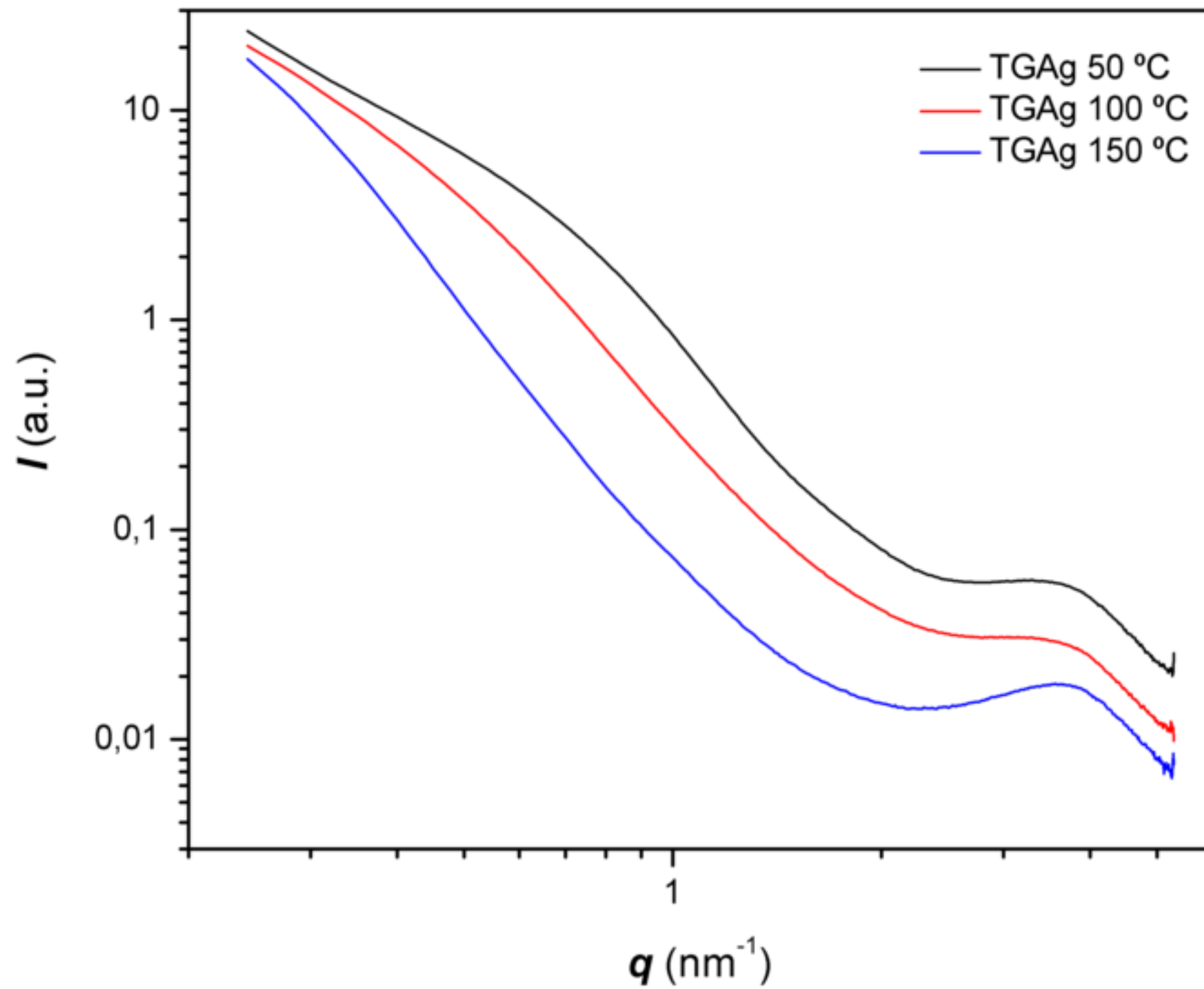
EDS Linear Scanning

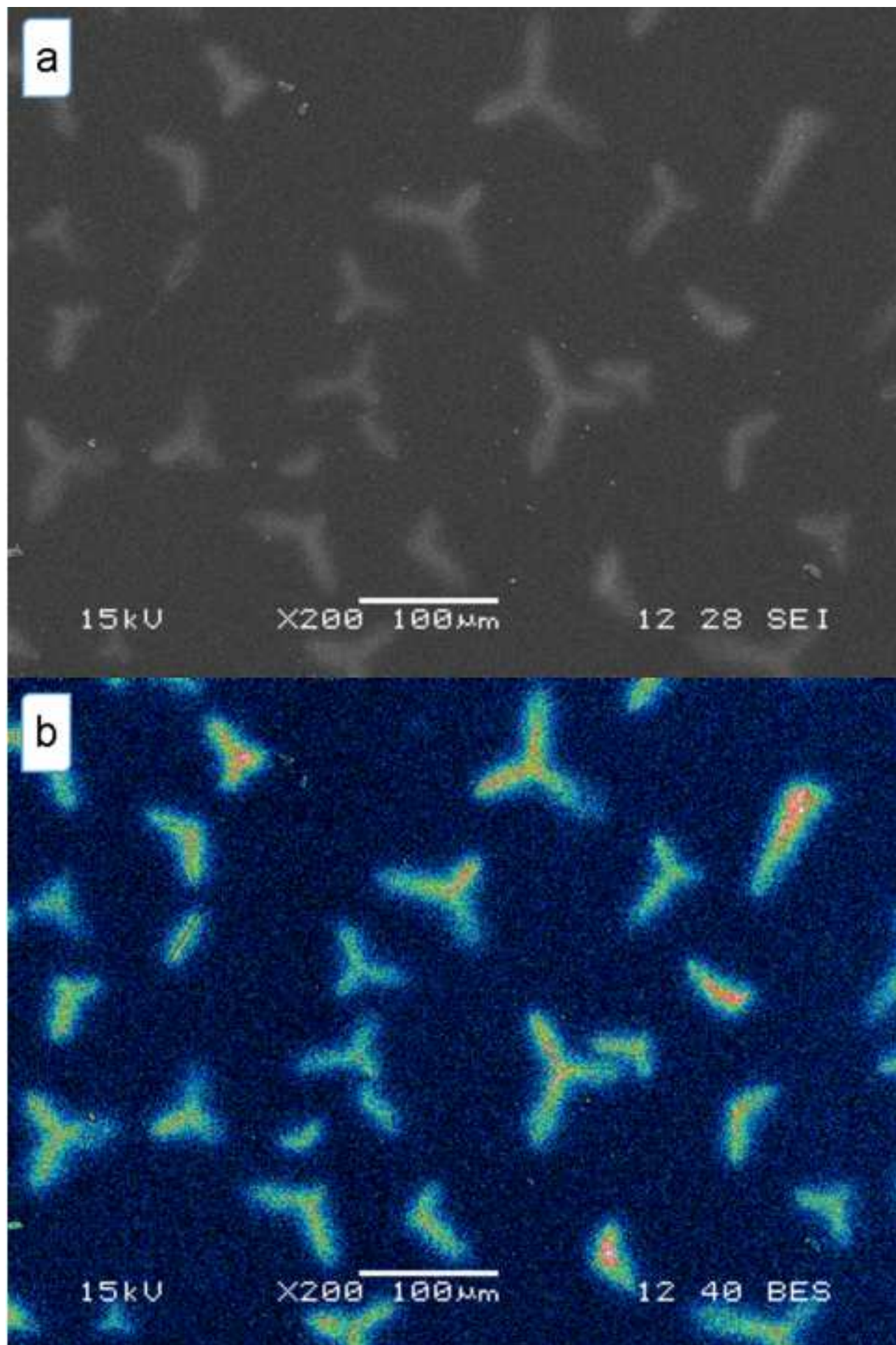


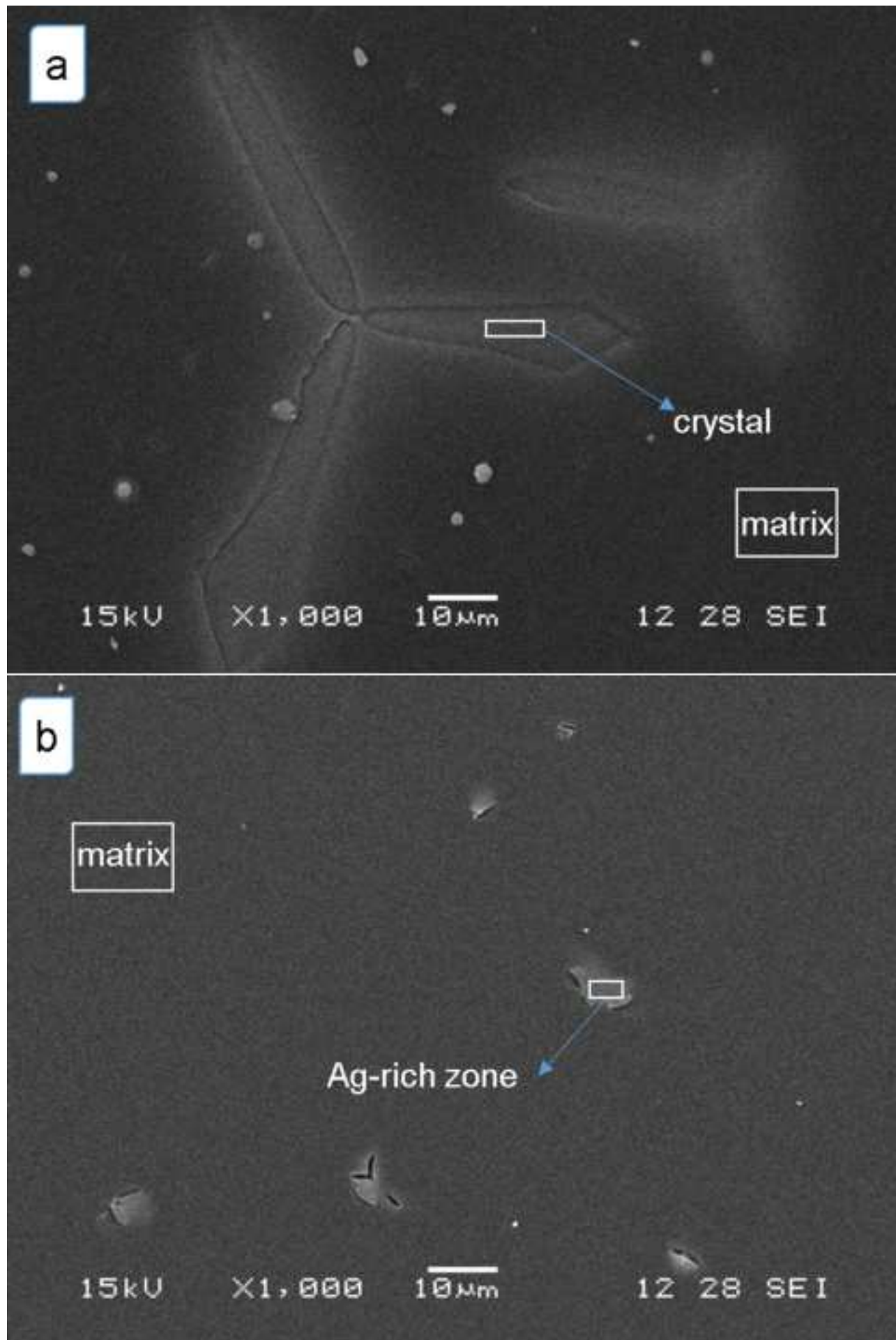
Electrochemical & Releasing properties

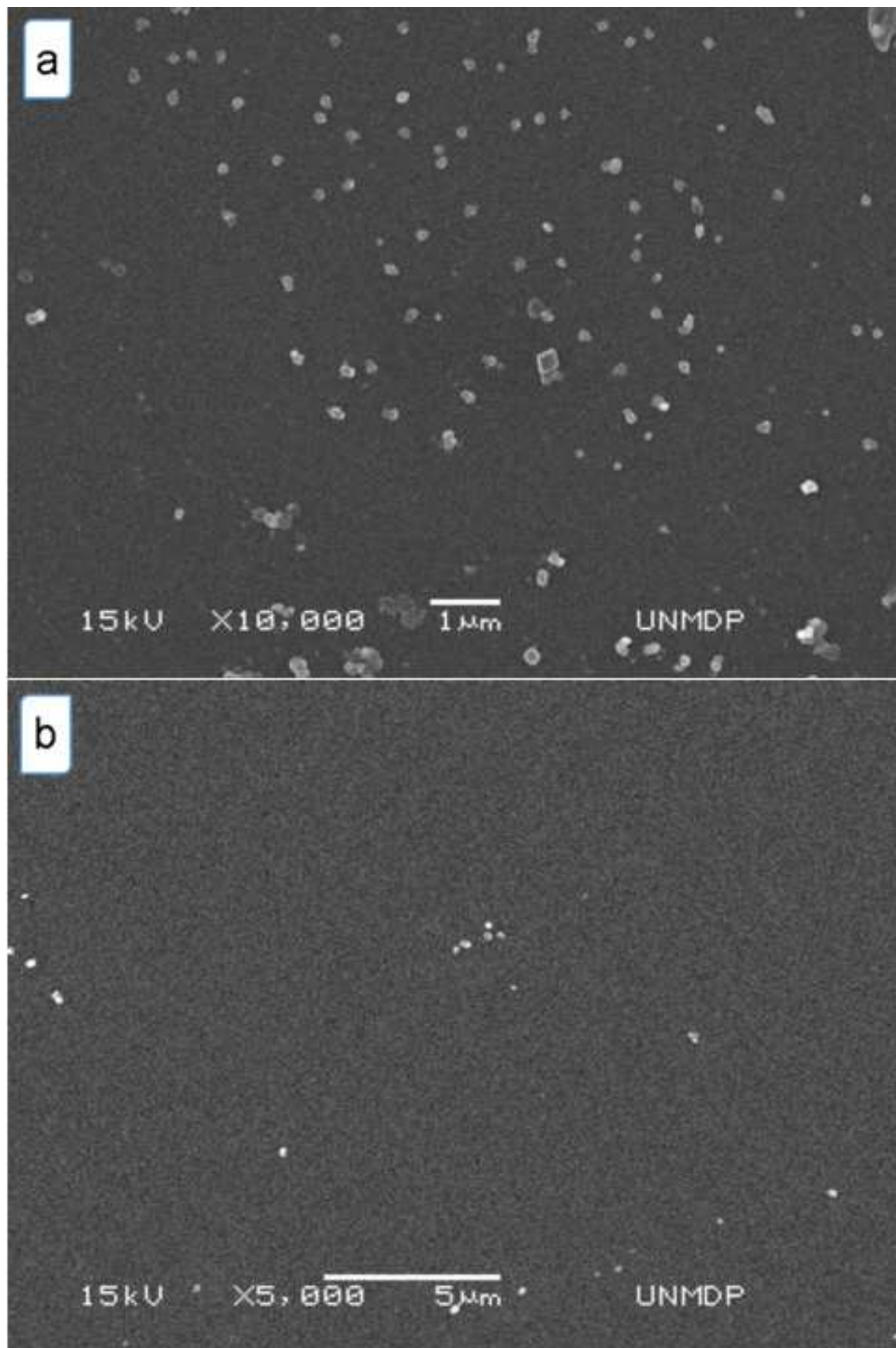


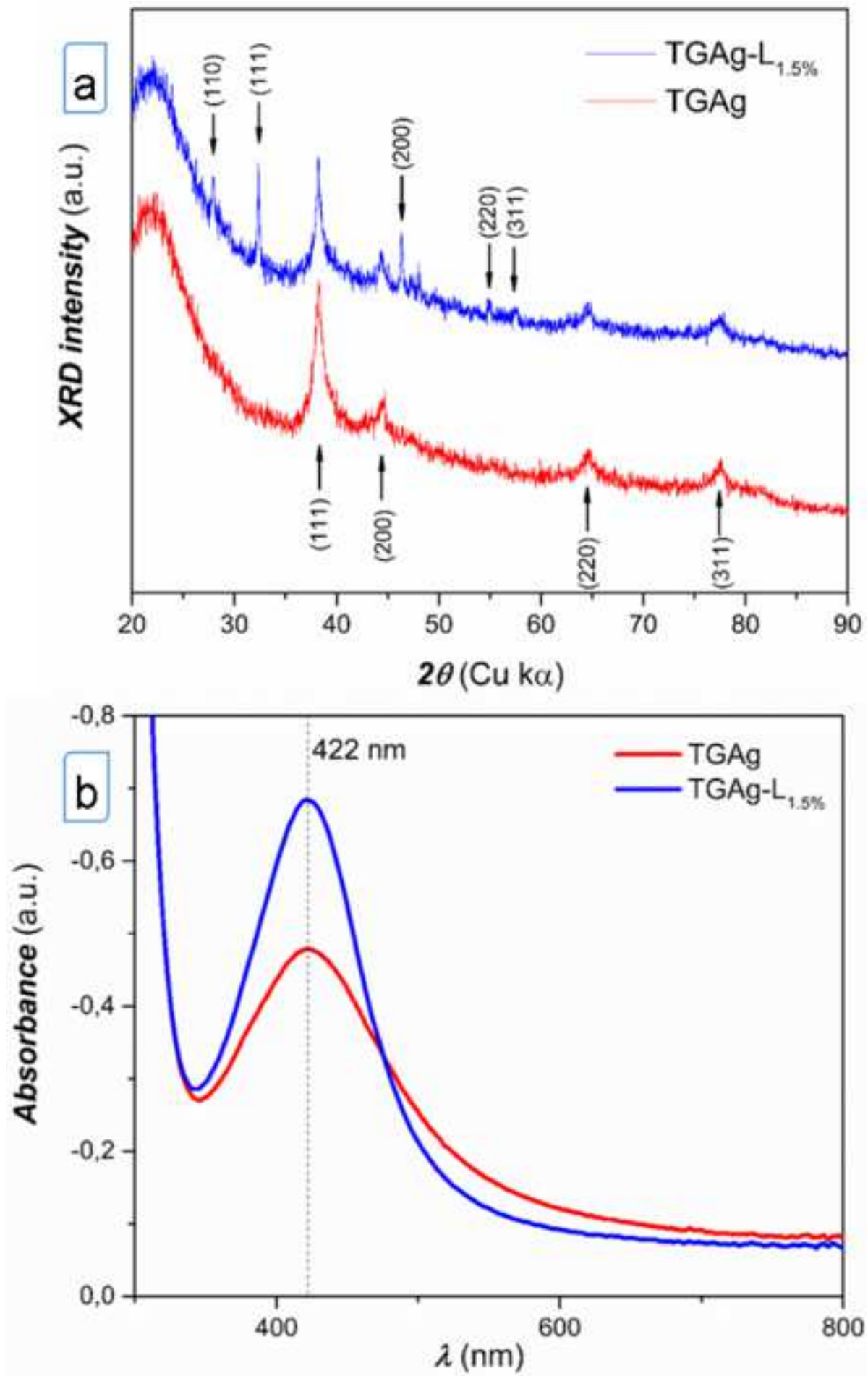


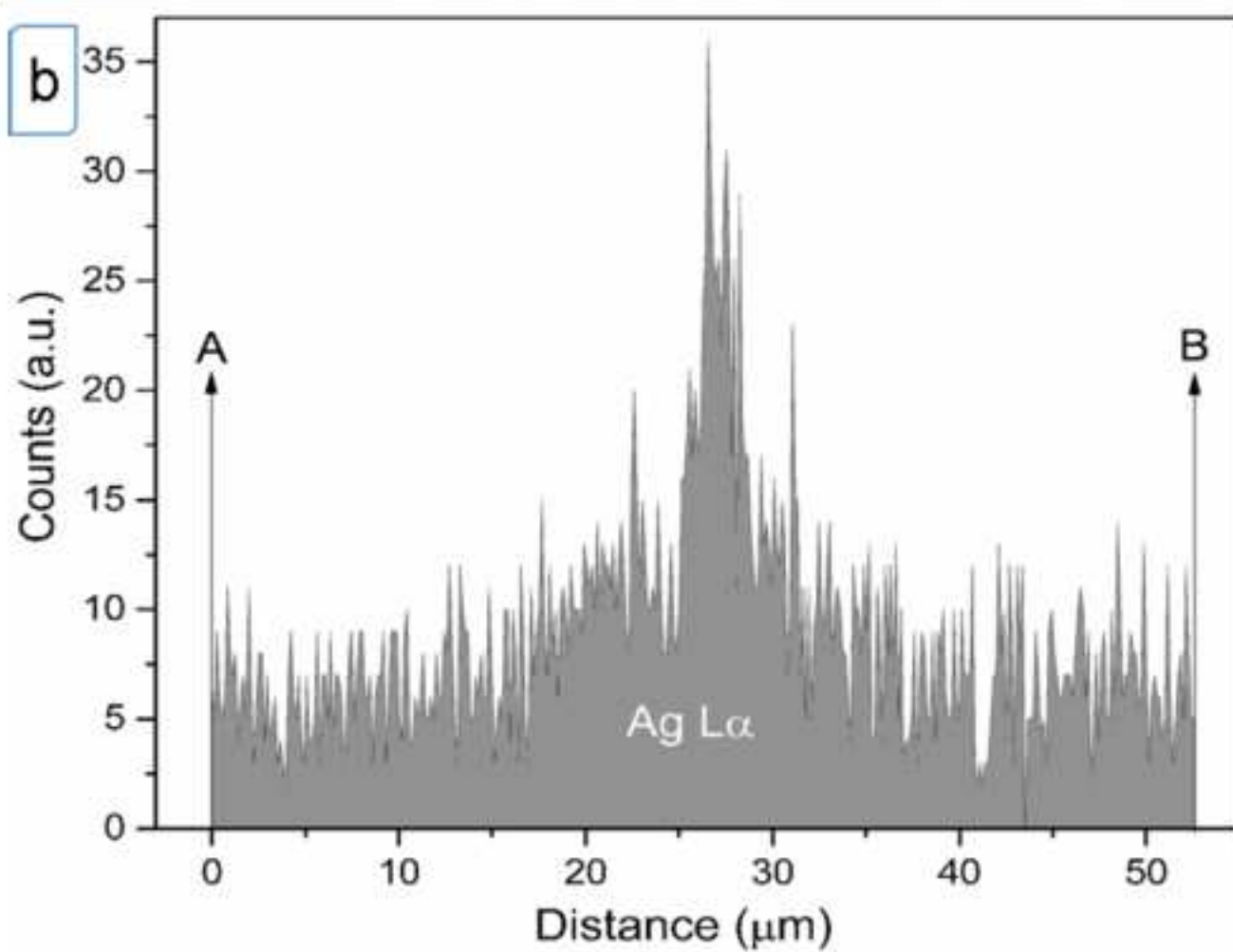
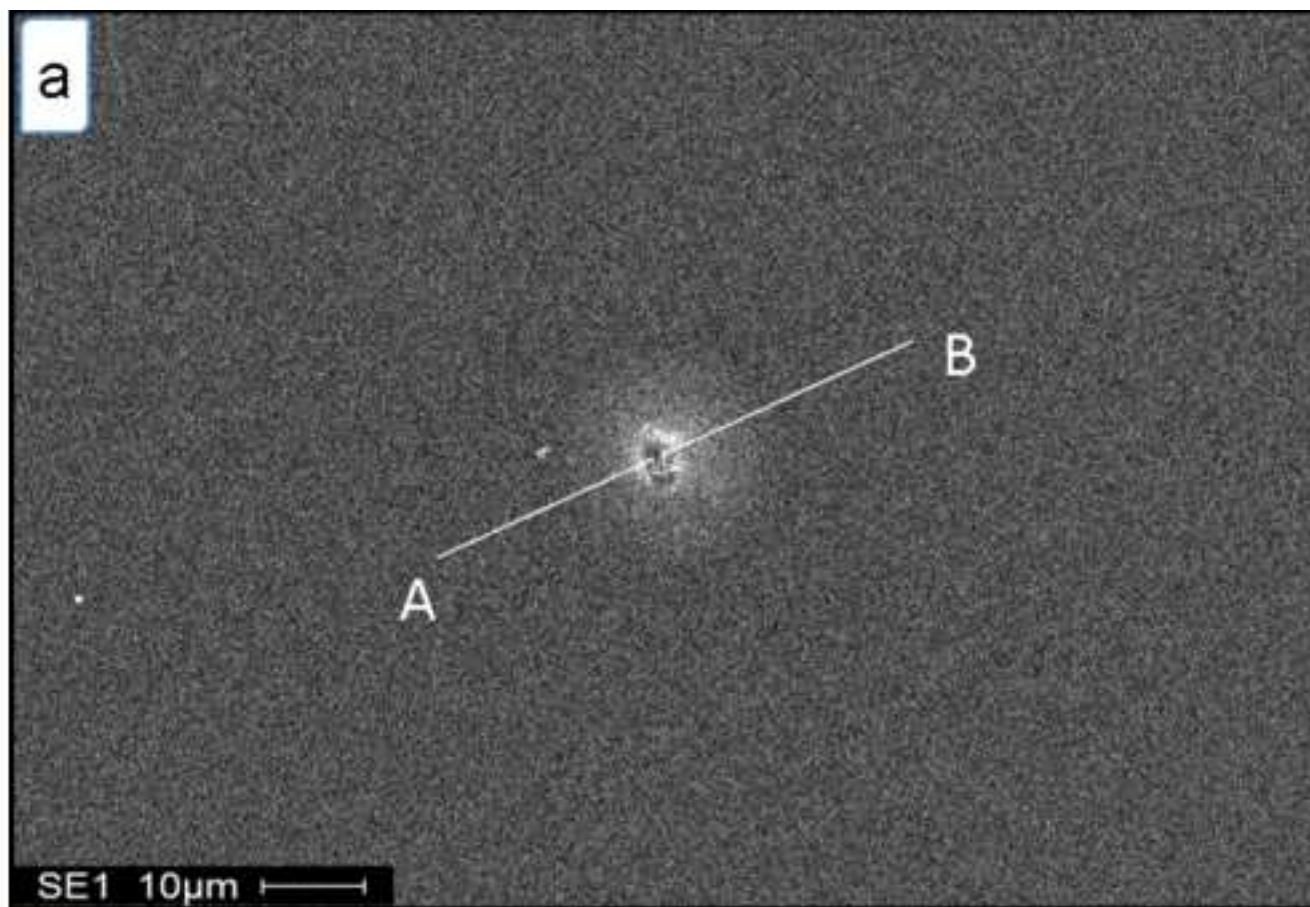


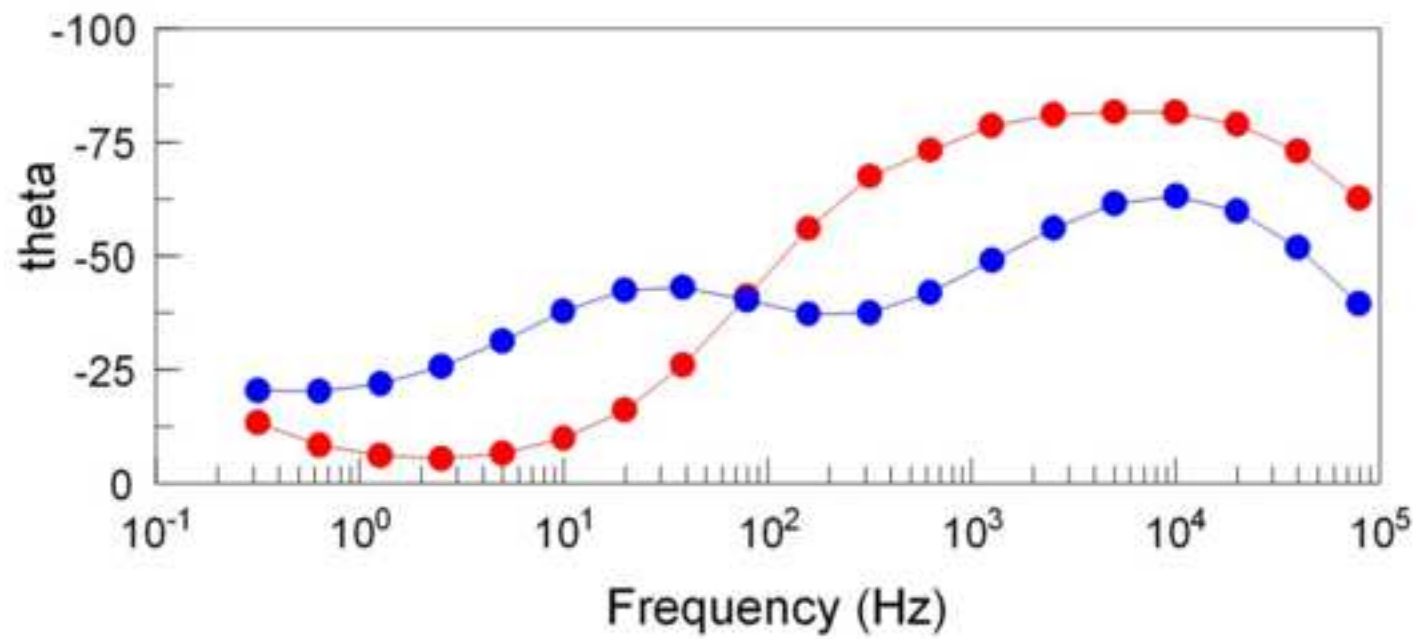
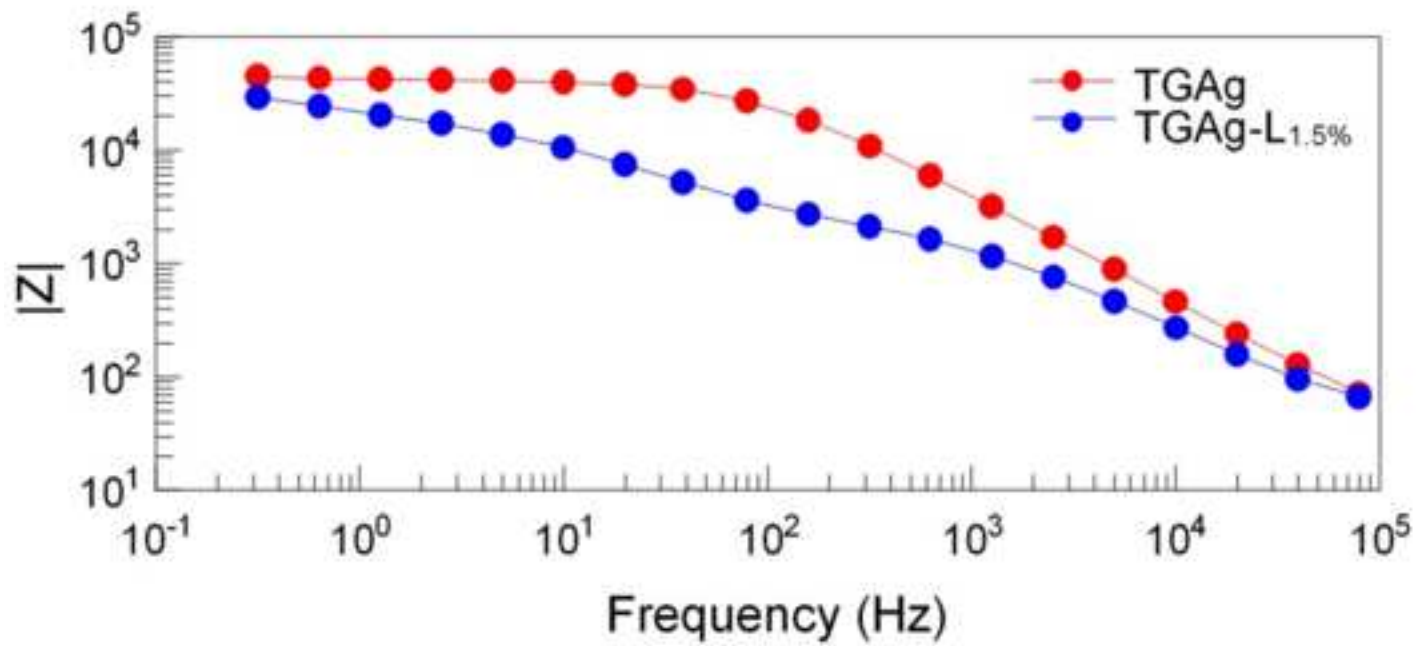


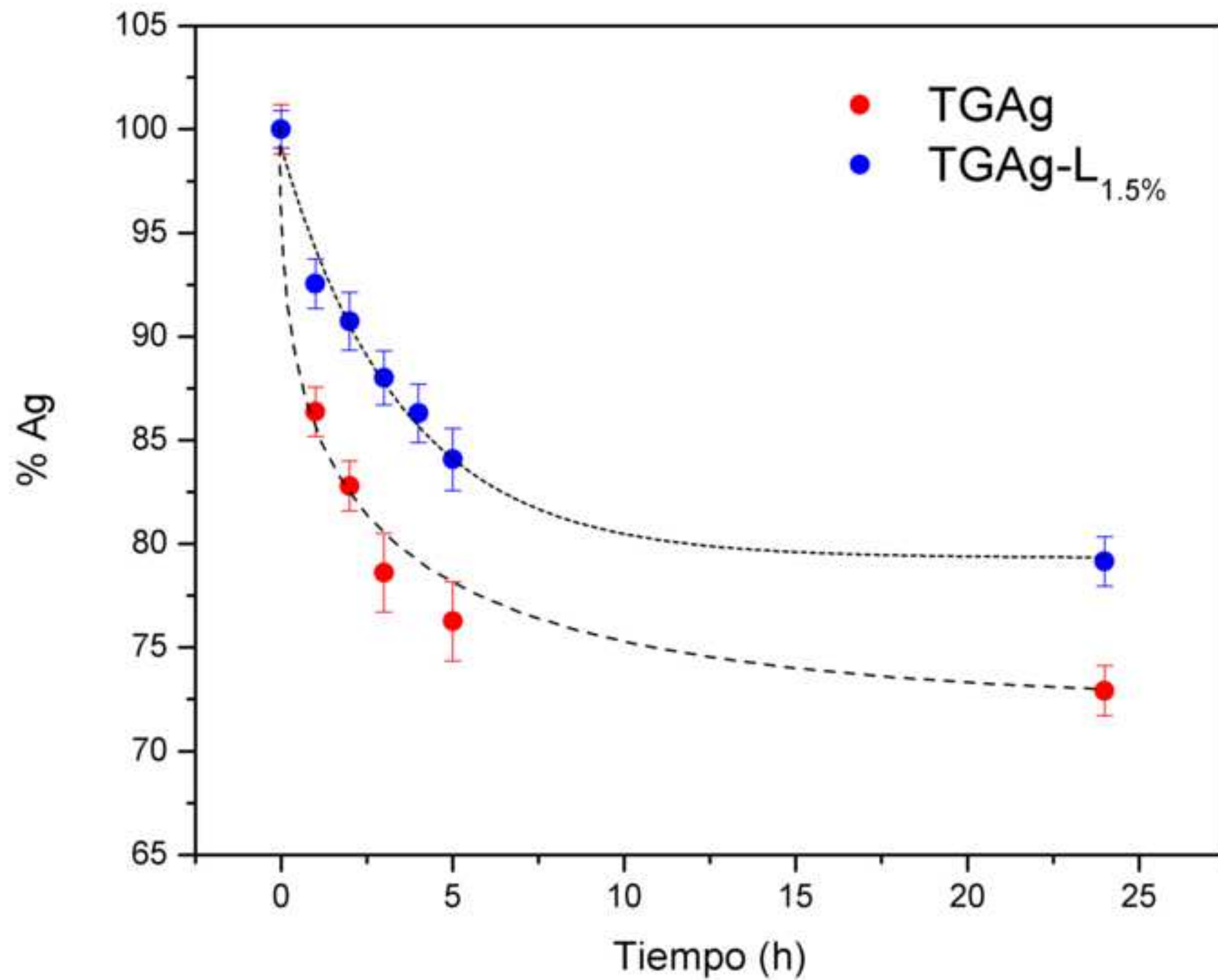












Element (At. %)	TGAg (RT)		TGAg-L _{1.5%} (RT)	
	Crystal	Matrix	Ag-rich zone	Matrix
C	31.14	26.76	30.93	34.13
O	33.34	39.84	37.38	37.09
Si	28.24	29.93	24.87	24.96
Na	1.71	1.12	3.22	1.48
Ca	0.90	0.87	1.07	0.92
Ag	2.37	0.05	1.02	0.35